Copy 641

[redacted]

NASA MEMO 5-11-59L

NASA MEMO 5-11-59L

[redacted]

CLASSIFICATION CHANGED
UNCLASSIFIED
TO
By Authority of NASA TD 71-445 Date 7-8-71

NASA

MEMORANDUM

Declassified by authority of NASA
Classification Change Notices No. 314
Dated ** 9-30-71

AN INVESTIGATION OF CLUSTERED JET-EXIT ARRANGEMENTS AT SUPERSONIC SPEEDS

By John M. Swihart and Arvid L. Keith, Jr.

Langley Research Center
Langley Field, Va.

FACILITY FORM 602

N71-74021 (ACCESSION NUMBER)	(THRU)
49 (PAGES)	None (CODE)
(NASA CR OR TMX OR AD NUMBER)	(CATEGORY)

[redacted]

NATIONAL AERONAUTICS AND SPACE ADMINISTRATION

WASHINGTON

June 1959

[redacted]

1E

[redacted]

NATIONAL AERONAUTICS AND SPACE ADMINISTRATION

MEMORANDUM 5-11-59L

AN INVESTIGATION OF CLUSTERED JET-EXIT ARRANGEMENTS AT SUPERSONIC SPEEDS*

By John M. Swihart and Arvid L. Keith, Jr.

L
4
2
2

SUMMARY

An investigation of several side-by-side clustered jet-exit configurations has been conducted in the Langley 9- by 12-inch blowdown tunnel at Mach numbers from 1.62 to 3.05. The semispan models were mounted from the tunnel wall, and the three jet exhausts were simulated with cold air. The angle of attack was maintained at 0° and the Reynolds number range was from 7×10^6 to 11×10^6 based on model wing root chord.

The results indicated that high negative base pressure coefficients were incurred whenever a blunt-base area was present, whether on the individual nacelle or between the engine nacelles. It was estimated that better performance might be obtained when the boattail angle was reduced and nozzle-area ratio was increased as long as the Mach number was within an increment of about 0.6 of the design Mach number, whereas greater amounts of overexpansion would probably result in performance losses.

INTRODUCTION

Research on the interference effects of jet-exhaust systems has been confined mainly to single-engine installations in which the jet-interference effects are associated only with the individual afterbody or control surfaces of the airplane. Information on the internal-flow phenomena of jet nozzles, the external-flow interferences of jet exits, and the combined internal-external flow on performance of single-engine installations is fairly well documented. (For example, see refs. 1 to 9.)

Large supersonic airplanes, however, may have a number of engines grouped together in a side-by-side arrangement. For such configurations,

[redacted]

[redacted]

interference of the multiple jets on the afterbodies, bases, and fairings between engines would be expected to have important effects on the airplane performance. Some preliminary results obtained with a side-by-side clustered exit arrangement at supersonic speeds are shown in reference 10.

The purpose of this paper is to present data obtained in the Langley 9- by 12-inch blowdown tunnel for several clustered exit arrangements which might be applicable to supersonic-bomber and transport designs. The semispan model simulated a propulsion system mounted below the wing with the jet exits at the wing trailing edge. The geometric jet-exit variables included nozzle-area ratio, boattail angle, base area, and fairing between nacelles. The jet flow was simulated with cold air at jet total-pressure ratios from 1 (jet-off) to about 40 over a Mach number range from 1.62 to 3.05. The Reynolds number range was from about 7×10^6 to 11×10^6 based on wing root chord. L 4 2 2

SYMBOLS

A area

d diameter

C_D drag coefficient, $\frac{D}{qS}$

$C_{D,i}$ jet-off drag coefficient of configuration 8 with the pressures on the base and jet-exit areas adjusted to free-stream static pressure

C_F thrust coefficient, $\frac{F}{qS}$

$C_{F,i}$ ideal thrust coefficient, $\frac{F_i}{qS}$

C_p pressure coefficient, $\frac{p_l - p_\infty}{q}$

D drag

F thrust

F_i ideal jet thrust for complete isentropic expansion to free-stream static pressure, $w\sqrt{\frac{2R}{g}\frac{\gamma}{\gamma - 1}T_{t,j}\left[1 - \left(\frac{p_\infty}{p_{t,j}}\right)^{\frac{\gamma-1}{\gamma}}\right]}$

L
4
2
2

g	acceleration of gravity
l	nozzle length from throat to exit
m	mass flow
M	free-stream Mach number
p	static pressure
p_t	total pressure
p_∞	free-stream static pressure
$p_{t,j}/p_\infty$	ratio of jet total pressure to free-stream static pressure
q	free-stream dynamic pressure
N_{Re}	Reynolds number
R	gas constant, ft/$^{\circ}$R
S	wing area (0.35 sq ft)
T_t	stagnation temperature
w	weight flow
x	distance from wing trailing edge (positive rearward)
β	boattail angle
γ	ratio of specific heats
ΔM	increment in free-stream Mach number
η	efficiency factor, $(C_F - C_D + C_{D,i})/C_{F,i}$
θ	nozzle divergence angle

Subscripts:

av	average
b	base

d	design
e	exit
i	ideal
j	jet
l	local
max	maximum
p	nozzle throat
t	total

L
4
2
2

APPARATUS AND METHODS

Models

The general jet-exit test arrangement is shown installed in the tunnel in figure 1. The basic model on which these jet-exit configurations were tested consisted of a semispan wing-fuselage configuration of a 6-engine supersonic bomber or transport airplane. (See figs. 1(c), 2, and 3.) The wing of the model was of a smaller scale than the engines to permit investigation of larger scale exits than would be possible with a true semispan model; however, the coefficients presented herein are based on the wing area of a true semispan model (0.35 sq ft) scaled according to exit size to give the drag coefficients realistic values. All the three jet-exit configurations studied were installed in a block detachable from the model; the block formed the afterbody of the model fuselage. Details of these configurations are shown in figure 4, and photographs are shown in figure 5. The fairing between engine afterbodies had the same shape for all configurations with the exception of configurations 8 and 9, which were solid-base models. (See figs. 2 to 5.)

Tests and Measurements

The tests were conducted in the Langley 9- by 12-inch blowdown tunnel at stagnation pressures from 35 to 50 lb/sq in. abs for Mach numbers of 1.62, 1.96, 2.55, and 3.05; the various Mach numbers were obtained by using interchangeable nozzle blocks. The test Reynolds number, based on model root chord of 10 inches, ranged from 7.1×10^6 to 10.8×10^6, depending upon the Mach number and stagnation pressure

of a particular test. The tests were conducted at angles of attack and yaw of 0°.

Air flow for the jet exits was furnished from a supply of 300 lb/sq in. abs and was piped to the model through the center of the strain-gage balance, as shown in figure 1. The air flow was turned 90° upon entering the model and exhausted axially through the three jet exits (fig. 1(c)). Jet total-pressure ratio $(p_{t,j}/p_{\infty})$ was controlled by a mechanical pressure-regulator valve, and total jet-weight flow was determined by a calibrated Venturi meter.

Jet total pressure was obtained from measurement of a total-pressure tube installed on the center line of each duct upstream of the throat. The Venturi meter was instrumented with a total-pressure tube and four manifold surface-pressure tubes, in accordance with American Society of Mechanical Engineers recommendations; a thermocouple was also installed in the downstream end of the meter to determine jet total temperature.

Surface-pressure orifices located as shown in figure 4 were used to determine the local-pressure coefficients over the fairing section between engine afterbodies. For model configurations with finite bases (configurations 2, 8, and 9), from 6 to 12 surface-pressure orifices were spaced in the base area to obtain base pressure coefficients.

Model forces and moments were determined by a three-component strain-gage balance with a hollow center which was attached to the tunnel top, as shown in figure 1(c). As mentioned previously, jet air was piped through the center of the balance to the model. The supply piping arrangement shown in figure 1 was selected to minimize force-interference effects between the model and the supply-pipe supports. Calibration of the balance with and without the supply pipe installed showed no effects of the pipe on the forces and moments within the accuracy of the measurements. The normal-force and pitching-moment outputs of the three-component balance were used to correct the axial-force output for interactions, and only axial-force data are presented in this paper.

Installation of the model through the tunnel wall required a clearance gap of 1/16 inch between the model and wall to avoid balance fouling. Because of the large differential in pressure existing between the atmosphere and the tunnel stream during operation at the higher Mach numbers, leakage flow through the gap and into the tunnel could cause significant interference effects on the measured forces and moments. In order to avoid these interference effects, a cylindrical shroud, the top of which was formed into a labyrinth seal, was installed around the balance. (See fig. 1(c).)

All pressure, temperature, and force data were recorded simultaneously and continuously during the period of each individual test point. Pressures were recorded on film using diaphragm-type pressure cells. The forces, moments, and jet total temperature were determined from the outputs of self-balancing potentiometers which were recorded on pen-type strip charts. The accuracy of measurement is estimated to be as follows:

M(1.62, 1.96, 2.55, and 3.05)	±0.02
$N_{Re}(7.1 \times 10^6$ to $10.8 \times 10^6)$, percent (caused by changes in T_t)	±0.01
T_t(510° to 540° R), °R	±2
$p_{t,j}/p_\infty$ (1 to about 40)	±0.4
C_D	±0.001
C_F	±0.001
C_p	±0.01

L
4
2
2

RESULTS AND DISCUSSION

Jet Simulation

Jet-exit flow for the present configurations was obtained using room-temperature air. The hot-jet parameters which affect the jet flow, therefore, obviously could not be simulated exactly. It is pointed out in reference 11, however, that the wave interference of hot and cold jets can be satisfactorily simulated if the initial slope of the jet boundary is duplicated. For example, the jet total-pressure ratio of configuration 9 operating at a Mach number of 3.05 would be 28.6 for the real hot-jet case ($\gamma = 1.27$). In order to duplicate the initial slope of this jet boundary, a jet total-pressure ratio of about 37 would be required with cold air ($\gamma = 1.40$) according to reference 11. Therefore, from this consideration and from a review of previous jet-simulation work (refs. 2, 5, 7, and 12), analysis figures presented in this paper, where data are plotted at scheduled pressure ratios for each Mach number, will be presented at the cold-air pressure ratio which produces almost the same jet boundary as the hot jet. (See fig. 6.)

Basic Data

The variation of measured thrust-minus-drag coefficient with jet total-pressure ratio for the configurations is shown in figure 7 at Mach numbers of 1.62, 1.96, 2.55, and 3.05. The value of $C_F - C_D$ plotted

at a jet total-pressure ratio of 1.0 represents the jet-off drag of the configuration. Force data are not available for configuration 7 at $M = 1.62$ or configuration 9 at $M = 3.05$.

Figure 8 shows the variation of pressure coefficients over the fairing between the nacelles of configuration 1 and configuration 4 with distance from the wing trailing edge. The differences in level and shape between the upper and lower surface pressure distributions are the result of the model geometry, and only the most rearward pressures were affected by the jets. Data have been shown for configurations 1 and 4 only, inasmuch as most of the models have contours between these two extremes. The exceptions are configurations 6, 8, and 9. As was expected, the pressures for boattailed nacelles such as configuration 1 have greater negative values than those for a cylindrical nacelle such as configuration 4. In general, increasing the jet total-pressure ratio produced more positive pressures at the wing trailing edge, particularly at pressure ratios greater than the nozzle design value. This effect would be expected, since the underexpanded jet would deflect the free stream and cause shock—boundary-layer interaction effects to move forward on the configuration. It is also noted that the effect of jet total-pressure ratios greater than the nozzle design value is more pronounced for configuration 4 than for configuration 1 (see $M = 2.55$ and 3.05), which is probably the result of the increased jet size. A similar effect of jet size has been shown in most of the reference data.

Base Pressures

The effect of jet total-pressure ratio on the average base-pressure coefficient is shown in figure 9 for configurations 2, 8, and 9 at the four test Mach numbers. Average values are presented inasmuch as the individual values were generally within ±0.01 of the average; however, for configurations 8 and 9, the values of base pressure coefficient for the most inboard tubes were generally more negative and were relatively unaffected by jet operation. The values for these tubes have been neglected in averaging the data. The effect of increasing the jet total-pressure ratio is similar for all configurations, and the trends of the data at $M = 1.62$ and 1.96 are similar to base pressure data obtained on single nacelles and clustered exits at transonic speeds (ref. 10). The value of the average base pressure coefficient becomes more positive as the Mach number is increased to 2.55 and 3.05, as would be expected since the pressure coefficient for full vacuum also increases with Mach number.

A comparison of the average base pressure coefficients for configurations 2, 8, and 9 is shown in figure 10 for a scheduled variation of jet total-pressure ratio with Mach number (fig. 6). This pressure-ratio schedule shown in figure 6 is considered to be typical for

turbojet engines designed for operation at Mach numbers of 3.0 and above. Configuration 9 experiences the most negative base pressure coefficients at Mach numbers below about 2.5. This result is believed due to the serious overexpansion of this nozzle at these Mach numbers and corresponding jet total-pressure ratios. For the higher Mach numbers at which configuration 9 begins operating at near design-pressure ratio, base pressures are less negative than those of configuration 8 (the zero-boattail flat-base model) and approach values of configuration 2 (the annular-base model). At Mach numbers slightly above those investigated, the larger jet of configuration 9 would cause even more interference on the base pressures, and $C_{p,b}$ of configuration 9 might become less negative than those of configuration 2.

L
4
2
2

It is of interest to note that if a configuration such as 9 were applied to an airplane with six 5-foot-diameter engine nacelles and a wing area of 6,000 sq ft, it would have a base-pressure-drag coefficient of 0.0003. If it is assumed that such an airplane would have a drag coefficient of 0.0130 at a Mach number of 3.0, the base-pressure-drag coefficient would increase the airplane drag coefficient by 2.3 percent. An increase of 2.3 percent in airplane drag does not look overly large; however, if this hypothetical airplane were a 125-passenger transport designed for cross-oceanic range, this drag increase would represent a loss of about six paying passengers. It should also be noted that the base area of configuration 9 is relatively small, and it was shown in reference 10 that configuration 8 (the zero-boattail, flat-base configuration) would have a base drag of about 7 percent of the total airplane trim drag. Configuration 8 was introduced as a reference model to permit the evaluation of the total cost of boattail and base drag on a supersonic airplane; and unless base bleed or some other device were used, the base drag of such a configuration would be very large. For one test at a Mach number of 3.05, a small quantity of base-bleed flow (1 percent of primary) was issued annularly around the three engines of configuration 8, and the drag coefficient decreased by a very small amount. No particular significance is attached to this result, but it is in the same direction and of about the same magnitude as the improvement in base pressure due to base bleed shown in reference 1.

Performance

The effect of Mach number on configuration efficiency factor η is shown in figure 11 for several configurations. Configuration efficiency factor η is defined as the measured thrust minus drag of the model plus the jet-off drag of the zero-boattail flat-base configuration (configuration 8), with the entire base region adjusted to free-stream static pressure, divided by the ideal thrust of a nozzle with the same throat diameter as the configuration being considered. In this manner, any change in drag due to boattailing, base area, internal nozzle separation,

or jet interference is reflected as an increase or decrease in the ideal thrust efficiency of the model.

Boattailing compared with base area.- Configurations 1, 2, and 8 are compared in figure 11(a) to show the effect of eliminating base area by boattailing. Each configuration has the same internal nozzle, and the data are compared for the jet-total-pressure-ratio schedule with Mach number shown in figure 6. It is indicated that configuration 1 (a 6° boattail model) is superior to configuration 8 (the zero-boattail flat-base model) over the entire Mach number range shown and is slightly better than configuration 2 (the annular-base model) at all Mach numbers. The lower η of configurations 2 and 8 is probably the result of the negative pressures experienced by the base annulus. It should be noted, however, that the overall boattailing of the configuration (boattail, base, and internacelle fairing) may be more important than the contour of the individual nacelle inasmuch as configuration 2 is almost as good as configuration 1, and the internacelle-fairing pressure distributions shown in figure 8 would be more favorable for configuration 2.

Effect of boattail abruptness.- The effect of boattail abruptness is shown in figure 11(b). Configurations 3 and 7 have the same internal nozzle contour but are boattailed in a different manner. (See fig. 4(b).) A comparison of these models indicates that the more gentle boattailing of configuration 3 is slightly better than the abrupt boattailing of configuration 7. The greater drag of configuration 7 is probably associated with a strong expansion over the 9° conical step ahead of the cylindrical afterbody (see fig. 4(b)); therefore, it appears to be advantageous to avoid regions of steep slope near the jet exits. In practice, neither of these external shapes would probably be used for cruising flight at $M = 3.0$, but they might be encountered in the Mach number range from about 1.6 to 2.2 when an all-variable-nozzle—afterbody combination would be increased in size during acceleration. The gentle boattailing of configuration 3 appears to be about 2.0 percent higher in η than configuration 7 in this speed range.

Nacelle boattail angle compared with nozzle-area ratio.- Several configurations are compared in figure 11(c) to illustrate the performance differences between nacelle boattail angle and nozzle-area ratio. The data are compared at jet total-pressure ratios corresponding to the schedule with Mach number shown in figure 6. The configurations presented in figure 11(c) would represent a scheduling of afterbody-nozzle geometry to produce optimum thrust at each point in the Mach number range. All configurations would represent maximum afterburner operation with the exit nozzle set for design pressure ratios from 6.6 (configuration 1), to 10.1 (configuration 3), and to 15.0 (configuration 4). Configuration 4 is superior to either 1 or 3 over the entire Mach number range of the investigation. It is to be expected that configuration 4 would be better at Mach numbers of 2.2 and above inasmuch as it has a zero-pressure-drag

nacelle, and the nozzle is at and above its design pressure ratio. The fact that configuration 4 is superior in a range where the nozzle is overexpanded is surprising and slightly encouraging. This fact would indicate that, for these nozzle lengths and this degree of overexpansion, it might be better to operate with an increased expansion ratio within $\Delta M = 0.6$ of design Mach number rather than to increase the drag with boattailing.

It is well known, however, that the off-design losses of high-pressure-ratio nozzles can be large (see ref. 14). It was suggested in reference 10 that, if a method could be found to eliminate these losses, perhaps a lightweight, uncomplicated nozzle could be built that would have desirable thrust characteristics over the entire Mach number range. Inasmuch as configuration 4 is superior to configurations 1 and 3 at Mach numbers as low as 1.62, perhaps some device such as the slotted afterbody or the terminal fairings described in references 9 and 13 could maintain a high level of thrust performance down into the transonic speed range. Another possibility might be the addition of large quantities of base-bleed or secondary flow when the nozzle is below design pressure ratio. (See ref. 14.) It should be noted, however, that the use of compromise nozzles to obtain good off-design performance may seriously affect the on-design range of a $M = 3.0$ cruise airplane.

L
4
2
2

Effect of increasing nozzle-area ratio.- Figure 11(d) is presented to show the effect of increasing nozzle-area ratio while keeping the external lines essentially constant. In these comparisons, note that the nozzle throat diameter is being decreased so that less thrust is being produced while the external drag remains essentially constant. A comparison of the data for configurations 1 and 5 (the 6° boattail models) indicates that at the lower Mach numbers the overexpansion in the nozzle of configuration 5 is very serious and causes losses of at least 10 percent in η near a Mach number of 1.62; however, as Mach number is increased, it becomes substantially better. The level of η near the design point ($M = 2.55$) of configuration 5 shows the desirability of increasing nozzle-expansion ratio to near ideal conditions, as might be done for an engine which has accelerated to design speed using maximum afterburning and can then maintain flight at partial afterburning.

Data for configuration 4 are compared with those of 9 on the same bases as configurations 1 and 5. Here, however, the comparison is not quite as valid as for configurations 1 and 5, since configurations 4 and 9 do not have the same external configuration between nacelles. With these differences in mind, the data indicate that the efficiency of configuration 9 is considerably lower than that of 4 at the lower Mach numbers (>2.5) which is probably a result of a combination of the drag on the blunt base between nacelles on 9 and the overexpansion of the nozzles. Unfortunately, no reliable force data were obtained for

configuration 9 at $M = 3.05$; however, the trend of the curve of η plotted against Mach number does seem to indicate that it will increase towards the design speed ($M = 2.75$) for configuration 9.

Flow Visualization

Figure 12 presents schlieren photographs obtained for some of the configurations during the investigation. Figure 12(a) shows configuration 1 at each test Mach number and corresponding jet total-pressure ratio. Figure 12(b) shows configurations 2, 6, 8, and 9 at a Mach number of 3.05 and a jet total-pressure ratio of about 32. The dark regions in the base of configurations 8 and 9 are an indication of expansion.

L
4
2
2

CONCLUDING REMARKS

An investigation of clustered jet-exit configurations arranged side-by-side along the trailing edge of a wing has been conducted in the Langley 9- by 12-inch blowdown tunnel at Mach numbers of 1.62, 1.96, 2.55, and 3.05. The results indicate that the overall boattailing of a clustered configuration may be more important than the boattailing of the individual nacelle; the better configurations were faired between nacelles. It was indicated that high negative base pressure coefficients were incurred whenever a physical base was present on the model, whether on the individual nacelle or between the nacelles. It was estimated that better performance might be obtained when the boattail angle was reduced and nozzle-area ratio increased as long as the Mach number was within an increment about 0.6 of the design Mach number, whereas greater amounts of overexpansion would probably result in performance losses.

Langley Research Center,
National Aeronautics and Space Administration,
Langley Field, Va., February 16, 1959.

REFERENCES

1. Cortright, Edgar M., Jr., and Kochendorfer, Fred D.: Jet Effects on Flow Over Afterbodies in Supersonic Stream. NACA RM E53H25, 1953.

2. Henry, Beverly Z., Jr., and Cahn, Maurice S.: Preliminary Results of an Investigation at Transonic Speeds to Determine the Effects of a Heated Propulsive Jet on the Drag Characteristics of a Related Series of Afterbodies. NACA RM L55A24a, 1955.

3. Falanga, Ralph A.: A Free-Flight Investigation of the Effects of Simulated Sonic Turbojet Exhaust on the Drag of a Boattail Body With Various Jet Sizes From Mach Number 0.87 to 1.50. NACA RM L55F09a, 1955. L 4 2 2

4. Greathouse, William K., and Beale, William T.: Performance Characteristics of Several Divergent-Shroud Aircraft Ejectors. NACA RM E55G21a, 1955.

5. Henry, Beverly Z., Jr., and Cahn, Maurice S.: Additional Results of an Investigation at Transonic Speeds To Determine the Effects of a Heated Propulsive Jet on the Drag Characteristics of a Series of Related Afterbodies. NACA RM L56G12, 1956.

6. Cubbage, James M., Jr.: Jet Effects on the Drag of Conical Afterbodies for Mach Numbers of 0.6 to 1.28. NACA RM L57B21, 1957.

7. Baughman, Eugene L., and Kochendorfer, Fred D.: Jet Effects on Base Pressures of Conical Afterbodies at Mach 1.91 and 3.12. NACA RM E57E06, 1957.

8. Rustemeyer, A. H., and Twomey, E. J.: Thrust and Drag Characteristics of Several Turbojet Exhaust Models at Supersonic and High Subsonic Mach Numbers. United Aircraft Corp. Report R-0922-16, (Contract NOa(S)55-134-C), Res. Dept., United Aircraft Corp., June 1957.

9. Swihart, John M., Norton, Harry T., Jr., and Schmeer, James W.: Effect of Several Afterbody Modifications Including Terminal Fairings on the Drag of a Single-Engine Fighter Model With Hot-Jet Exhaust. NASA MEMO 10-29-58L, 1958.

10. Swihart, John M., and Nelson, William J.: Performance of Multiple Jet-Exit Installations. NACA RM L58E01, 1958.

11. Love, Eugene S., Woodling, Mildred J., and Lee, Louise P.: Boundaries of Supersonic Axisymmetric Free Jets. NACA RM L56G18, 1956.

12. Runckel, Jack F., and Swihart, John M.: A Hydrogen Peroxide Hot-Jet Simulator For Wind-Tunnel Tests of Turbojet-Exit Models. NASA MEMO 1-10-59L, 1959.

13. Runckel, Jack F.: Preliminary Transonic Performance Results for Solid and Slotted Turbojet Nacelle Afterbodies Incorporating Fixed Divergent Jet Nozzles Designed for Supersonic Operation. NASA MEMO 10-24-58L, 1958.

14. Beheim, Milton A.: Off-Design Performance of Divergent Ejectors. NACA RM E58G10a, 1958.

CONFIDENTIAL

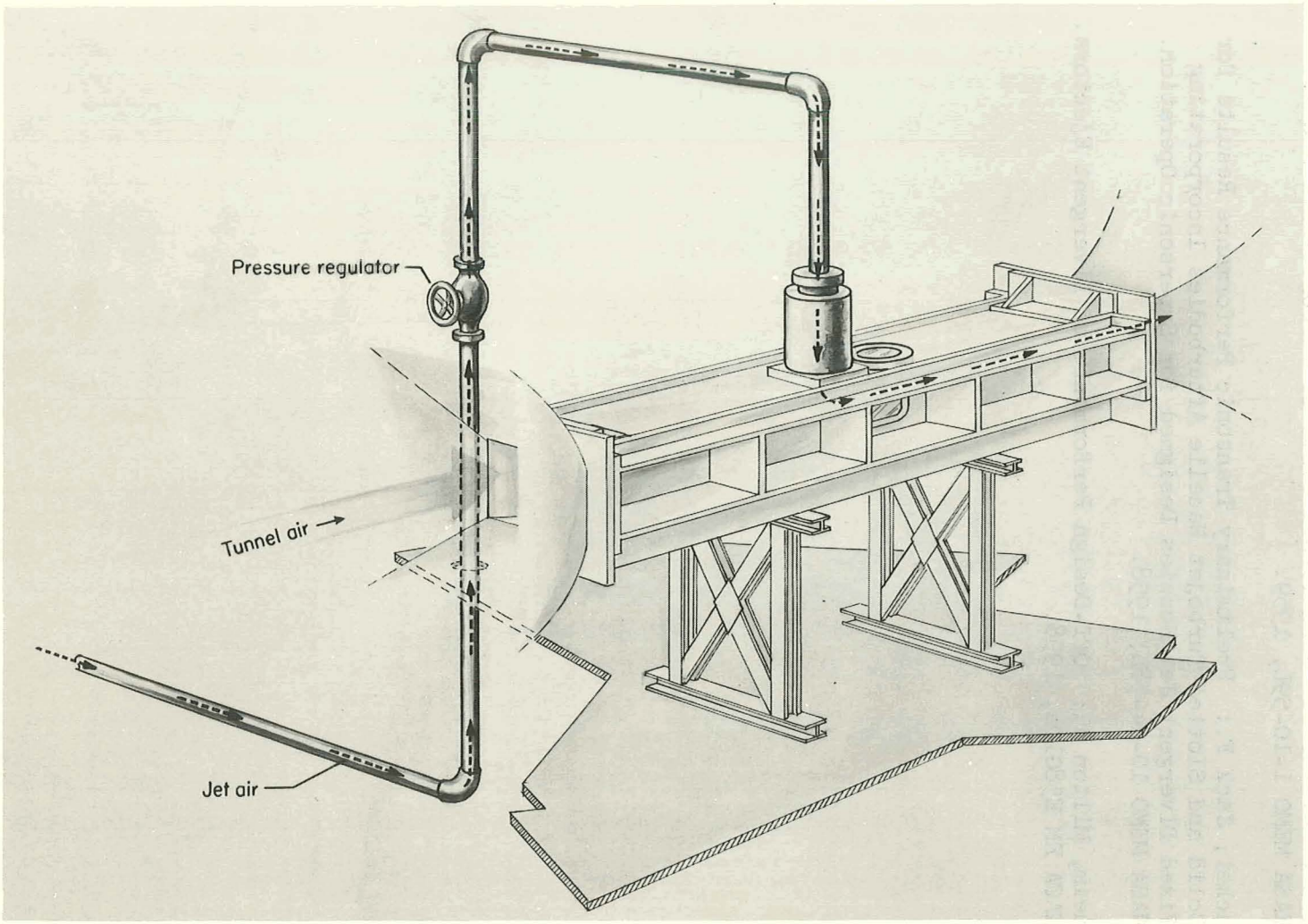

(a) Jet-air-supply piping and general view of tunnel. L-58-3607.1

Figure 1.- General test arrangement.

CONFIDENTIAL

CONFIDENTIAL

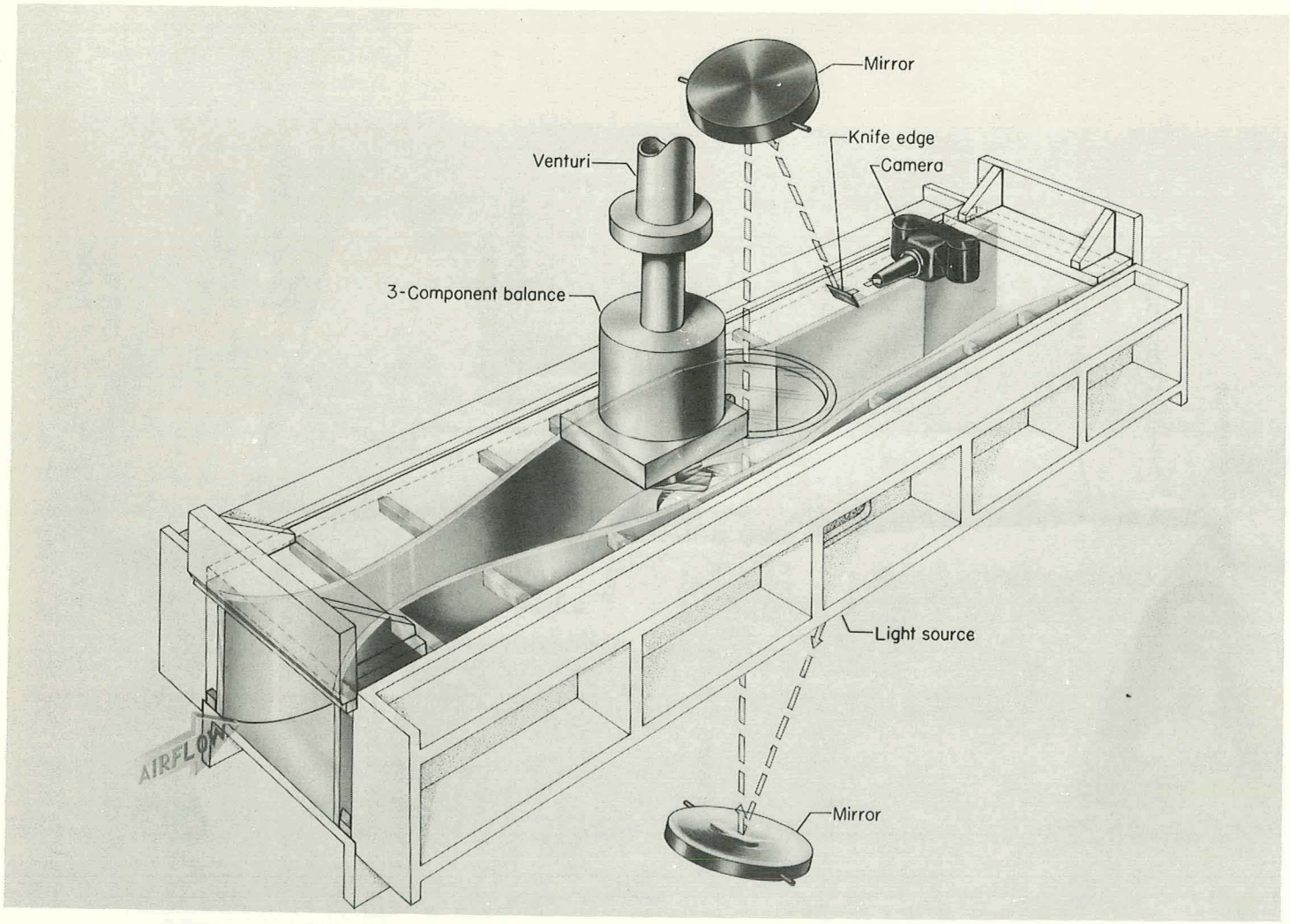

(b) 9- by 12-inch tunnel, balance arrangement, and schlieren setup. L-58-3606

Figure 1.- Continued.

CONFIDENTIAL

CONFIDENTIAL

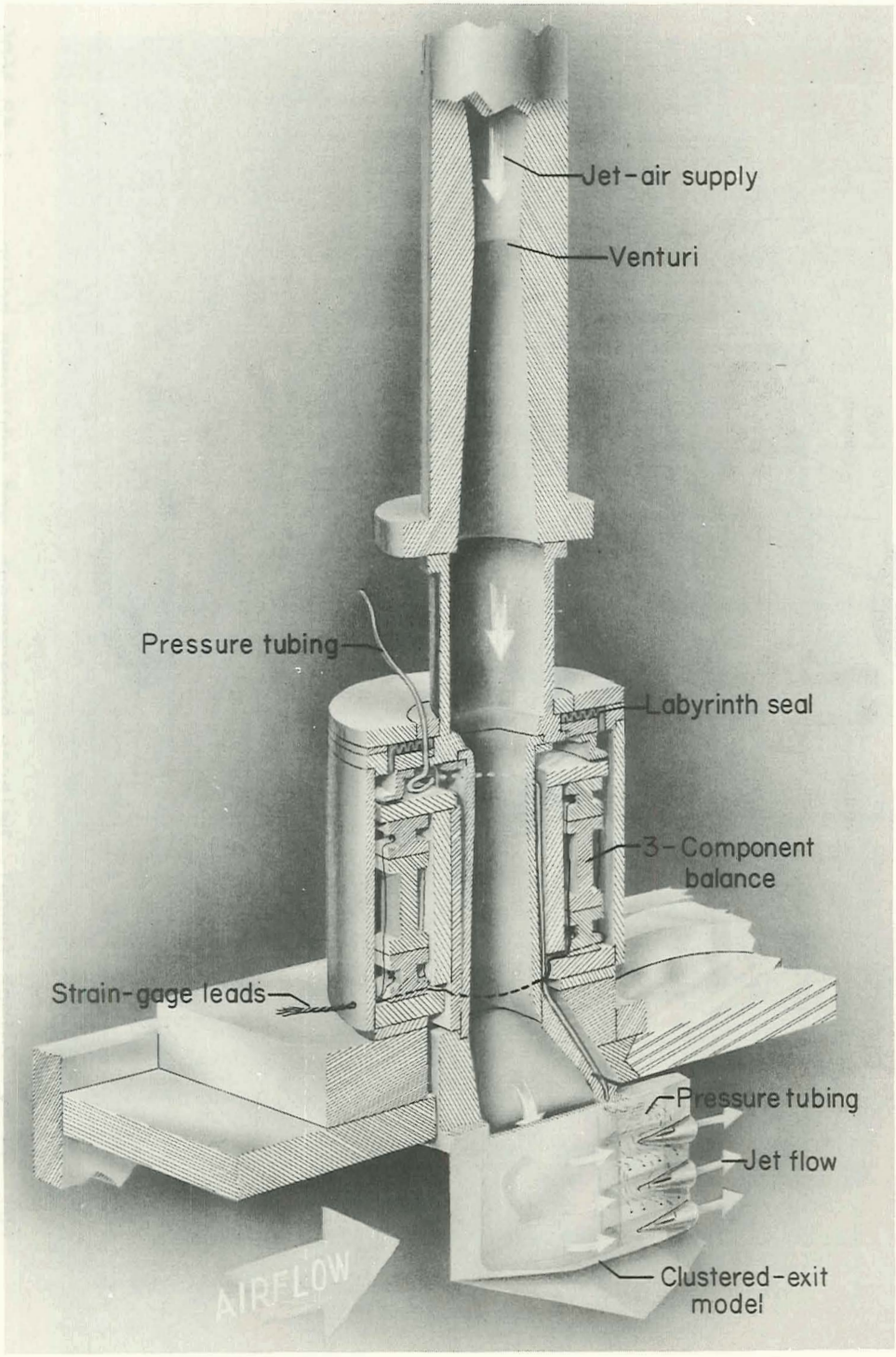

L-422

(c) Model installation. L-58-3605

Figure 1.- Concluded.

CONFIDENTIAL

L-422

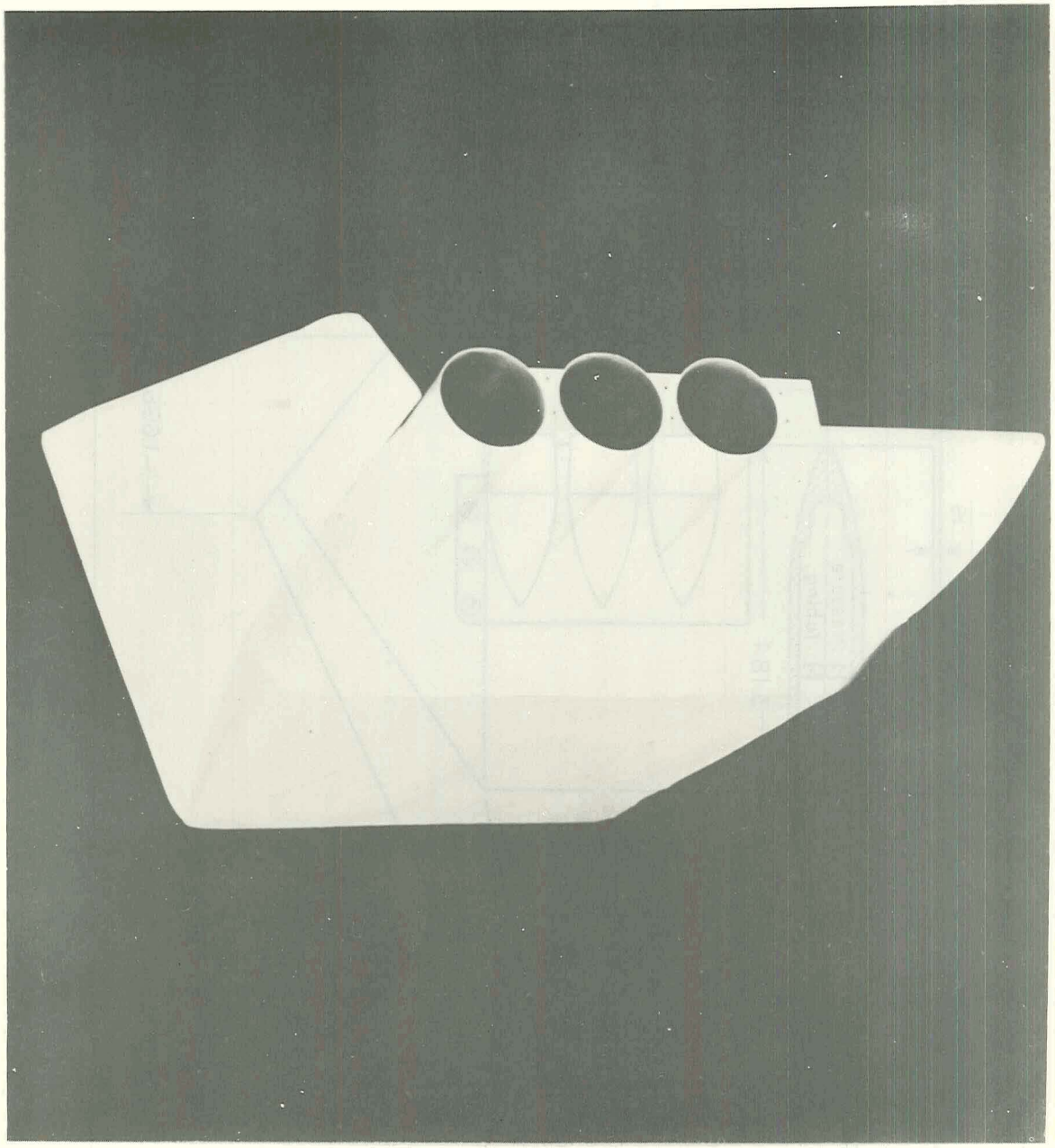

L-58-3780.1

Figure 2.- Photograph of complete model with configuration 9 installed.

CONFIDENTIAL

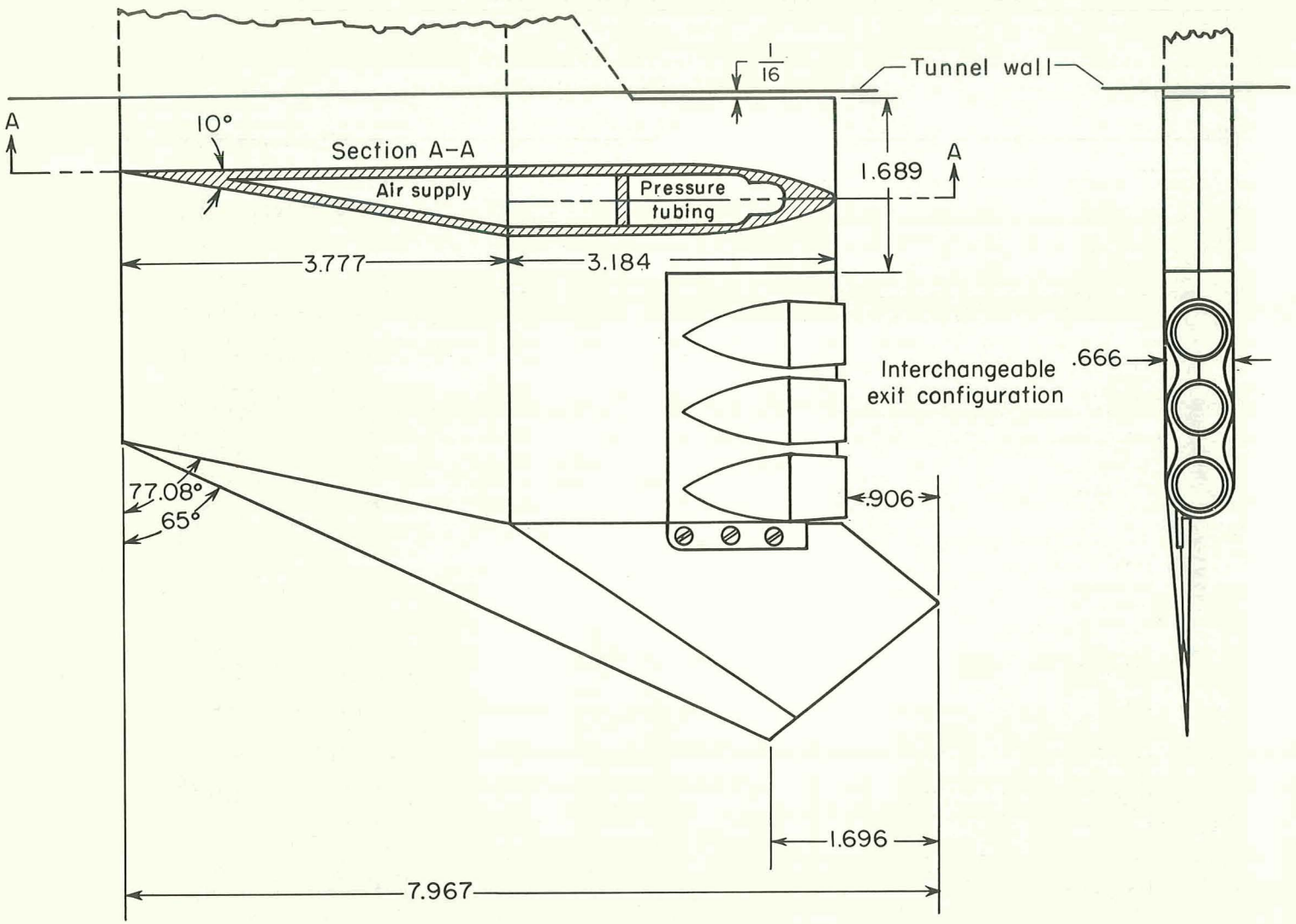

Figure 3.- Geometric details of clustered exit model. All dimensions in inches.

CONFIDENTIAL

CONFIDENTIAL

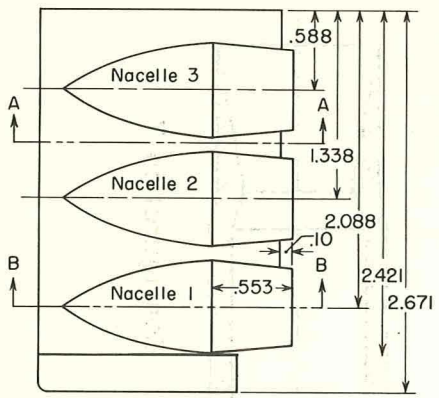

Configuration 1

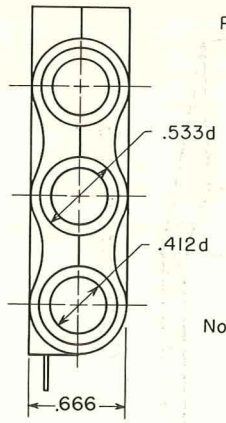

PRESSURE ORIFICE LOCATIONS

Config. 1 to 7

Wing upper and lower surface between nacelles 2 and 3

x	$x/d_{p,1}$
0.00	0.000
−.25	−.607
−.50	−1.215
−.75	−1.821
−1.00	−2.426
−1.25	−3.032

Note: A pressure orifice is also located at x = 0 between nacelles 1 and 2.

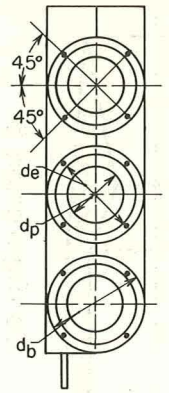

Base pressure orifices

Configuration 2

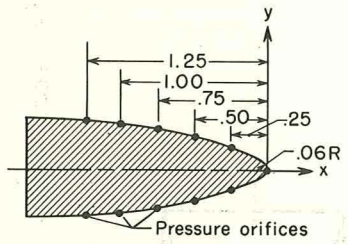

Section A–A

ORDINATES FOR FAIRING BETWEEN NACELLES

Config. 1 to 7	
x	y
0.00	0.000
−.16	.104
−.32	.160
−.48	.208
−.64	.248
−.80	.280
−.96	.303
−1.12	.320
−1.28	.328
−1.44	.333

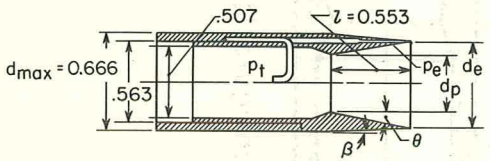

Section B–B

NOZZLE GEOMETRY									
Config	β	θ	d_p	d_e/d_p	l/d_p	d_b/d_e	d_e/d_{max}	Design $p_{t,j}/p_\infty$ Cold air $\gamma = 1.4$	Design $p_{t,j}/p_\infty$ Hot exhaust $\gamma = 1.27$
1	6.86	6.24	0.412	1.29	1.34	1	0.80	7.7	6.6
2	0.00	6.24	.412	1.29	1.34	1.25	.80	7.7	6.6
3	3.42	9.65	.412	1.46	1.34	1	.90	11.8	10.1
4	0.00	12.93	.412	1.62	1.34	1	1.00	16.8	15.0
5	6.86	16.62	.300	1.78	1.84	1	.80	22.9	18.8
6	15.56	3.00	.300	1.19	1.84	1	.54	5.3	5.0
7	9.00	9.65	.412	1.46	1.34	1	.90	11.8	10.1
8	0.00	6.24	.412	1.29	1.34	1.25	.80	7.7	6.6
9	0.00	12.00	.356	1.87	2.05	1	1.00	27.1	22.0

(a) Nozzle geometry and pressure-orifice locations.

Figure 4.- Details of interchangeable exit configurations.

CONFIDENTIAL

CONFIDENTIAL

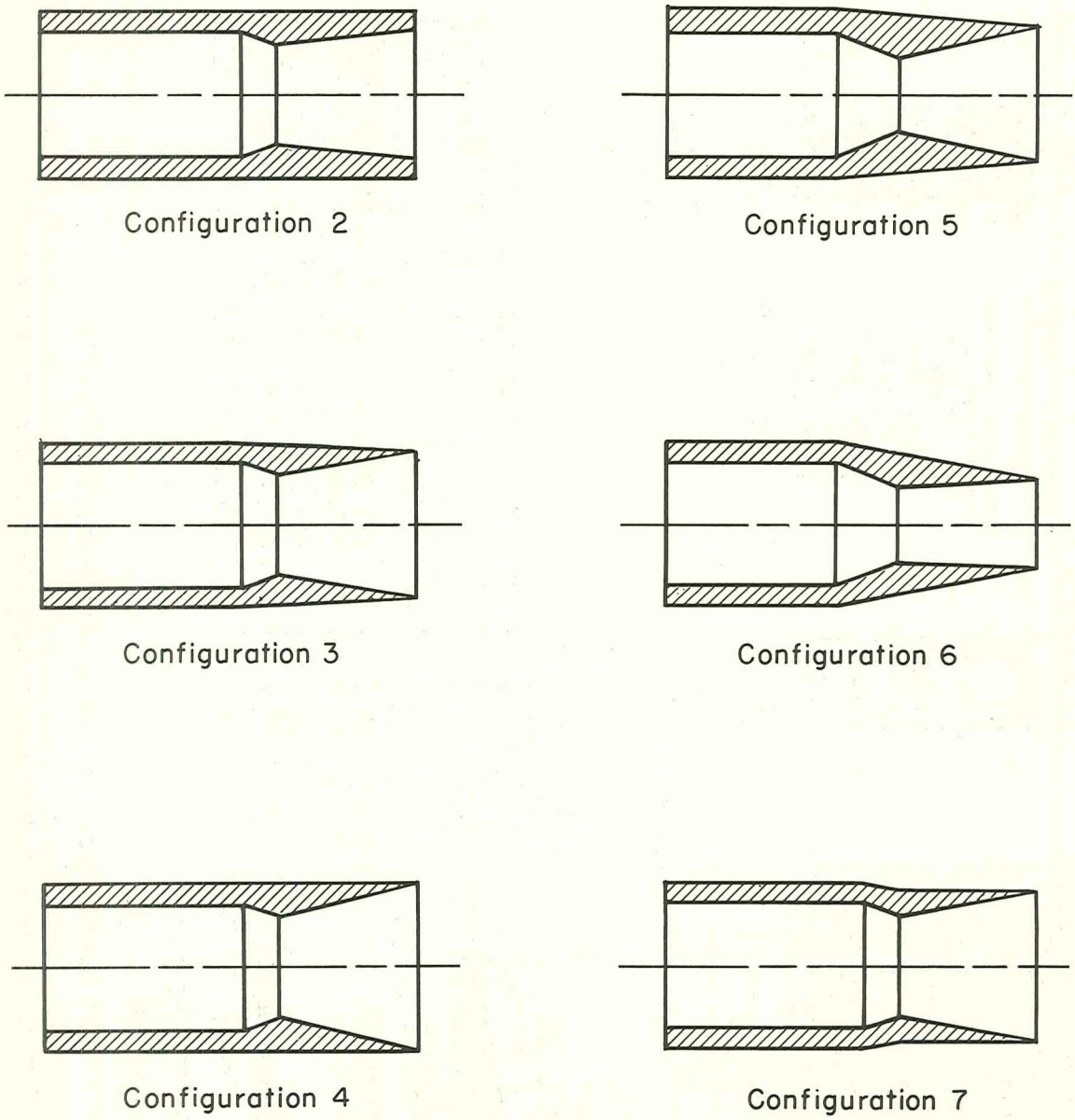

(b) Nozzle cross sections.

Figure 4.- Continued.

L-422

CONFIDENTIAL

L-422

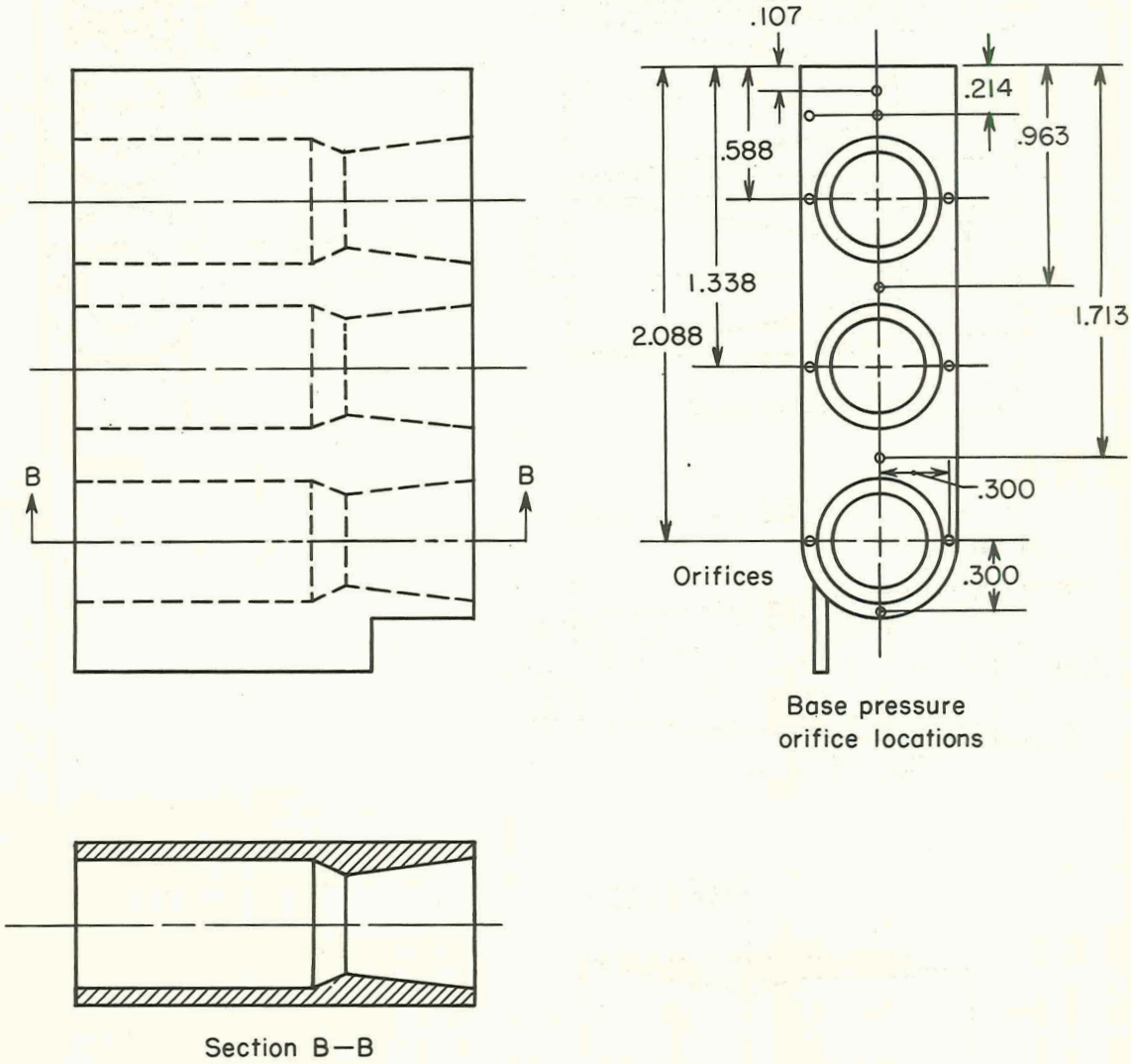

(c) Pressure-orifice locations of configuration 8.

Figure 4.- Continued.

CONFIDENTIAL

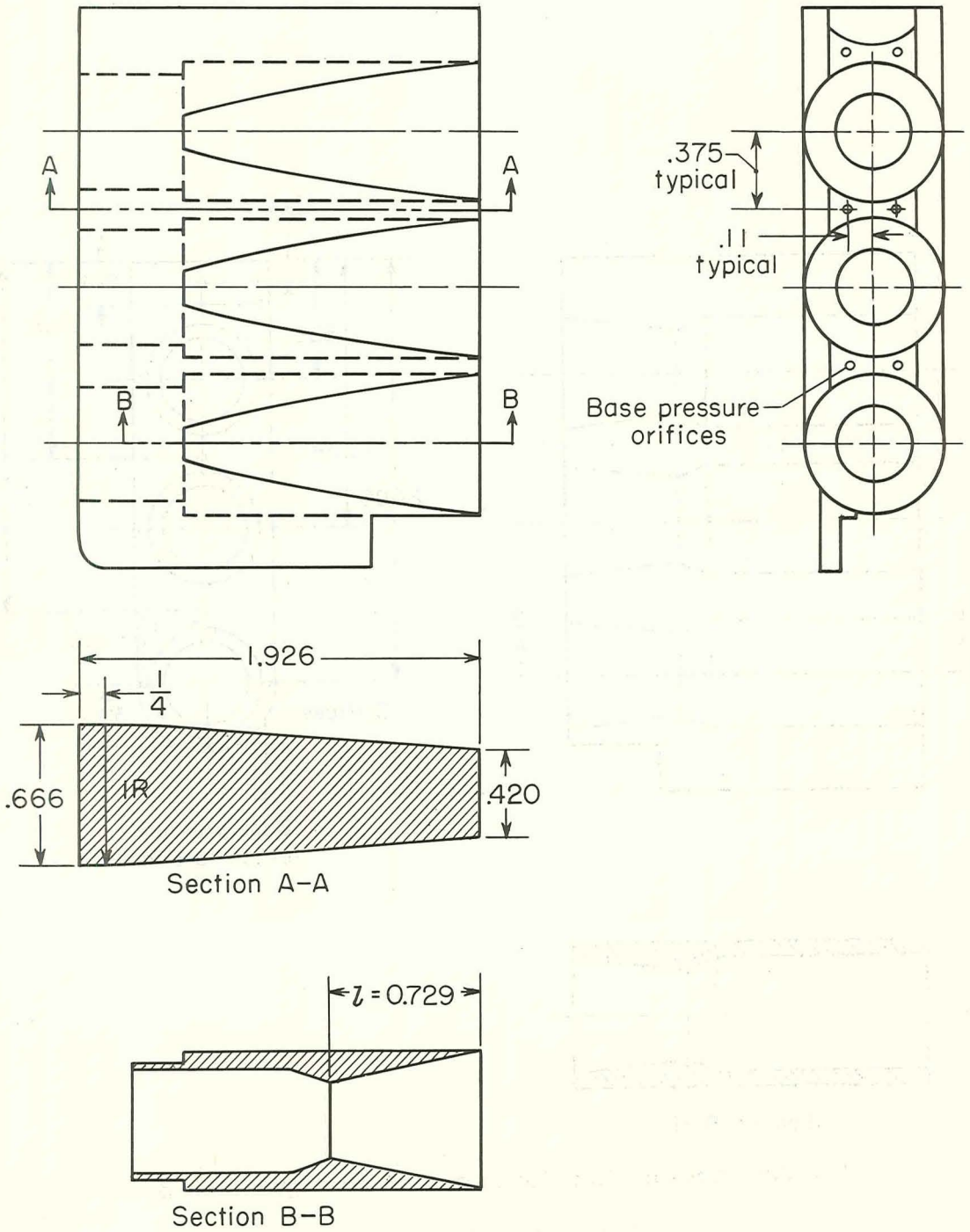

(d) Pressure-orifice location of configuration 9.

Figure 4.- Concluded.

CONFIDENTIAL

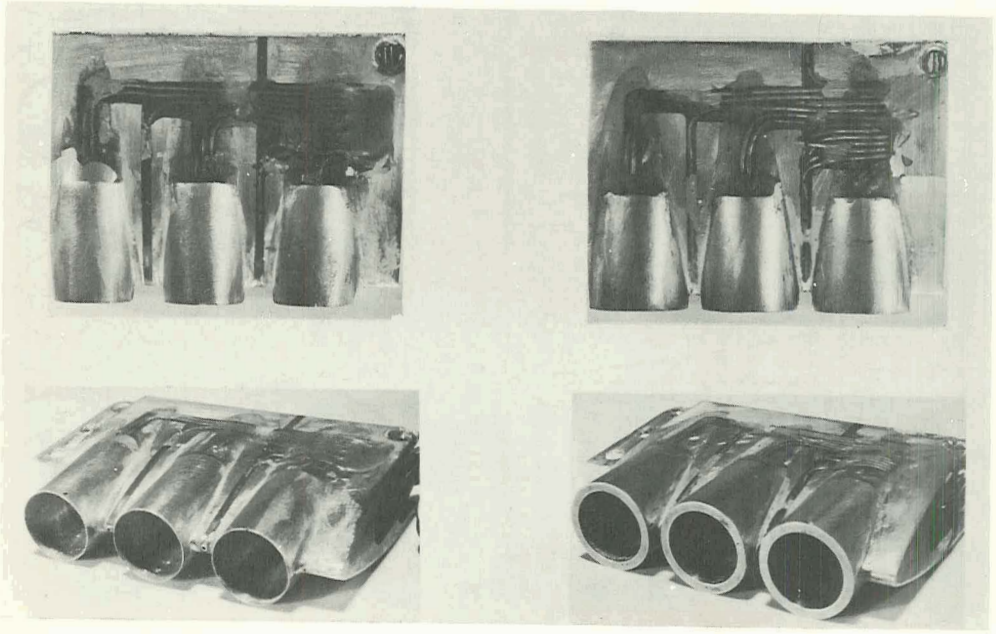

Configuration 1 Configuration 2

L-58-30

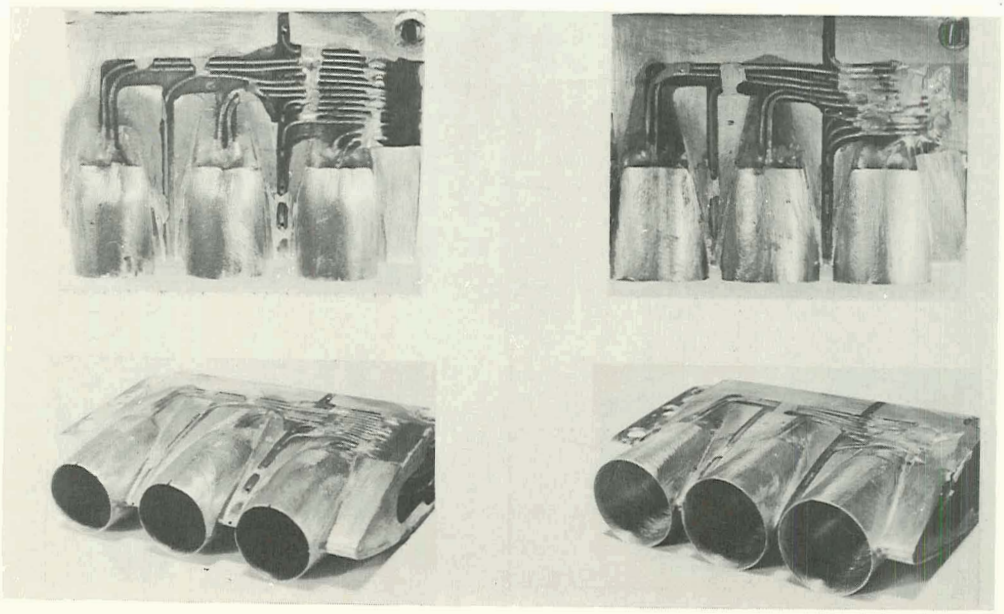

Configuration 3 Configuration 4

(a) Configurations 1 to 4. L-58-31

Figure 5.- Photographs of clustered exit configurations.

CONFIDENTIAL

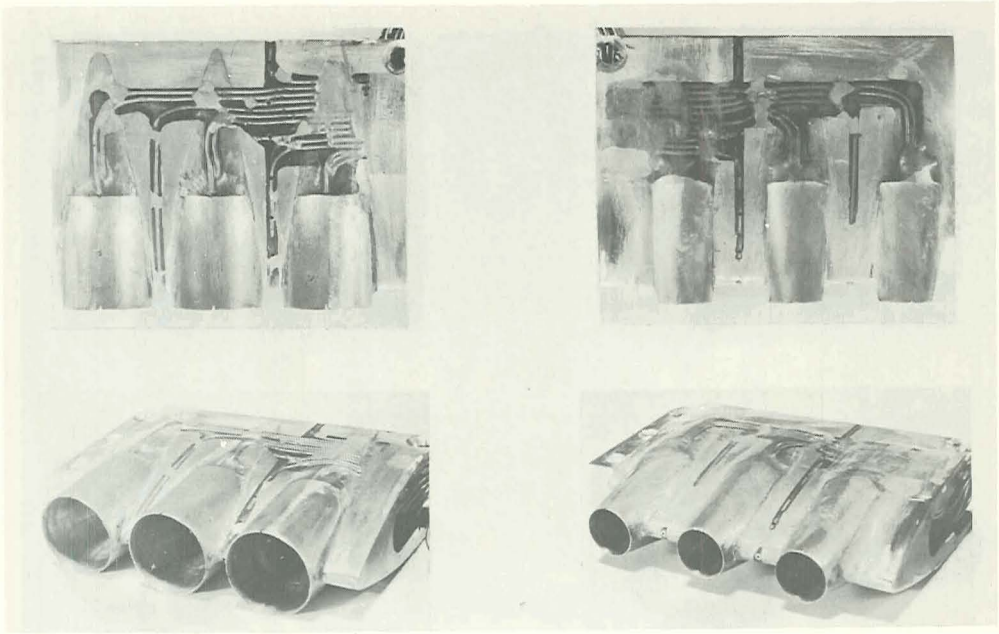

Configuration 5 Configuration 6

L-58-32

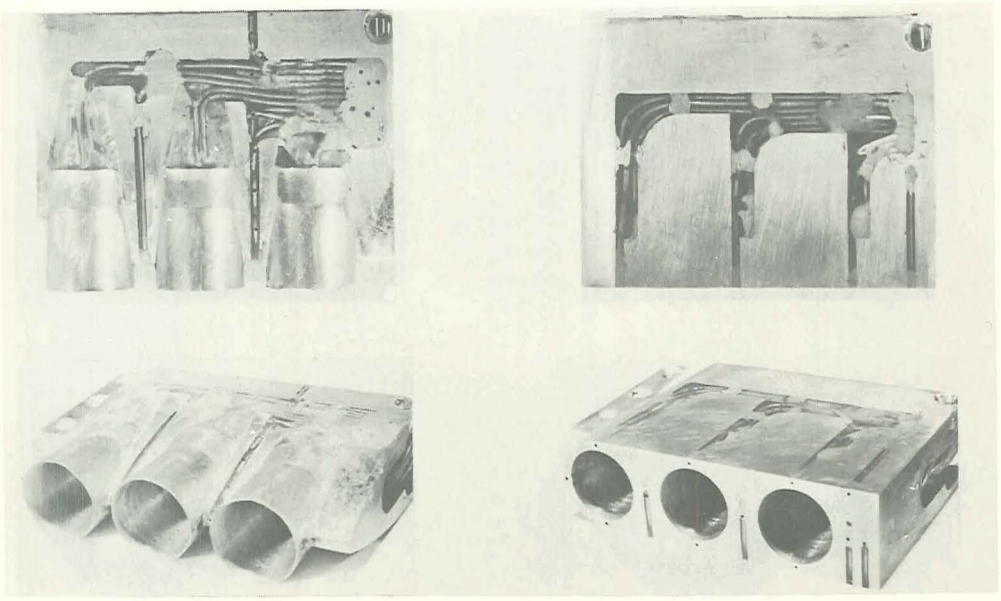

Configuration 7 Configuration 8

(b) Configurations 5 to 8. L-58-33

Figure 5.- Concluded.

CONFIDENTIAL

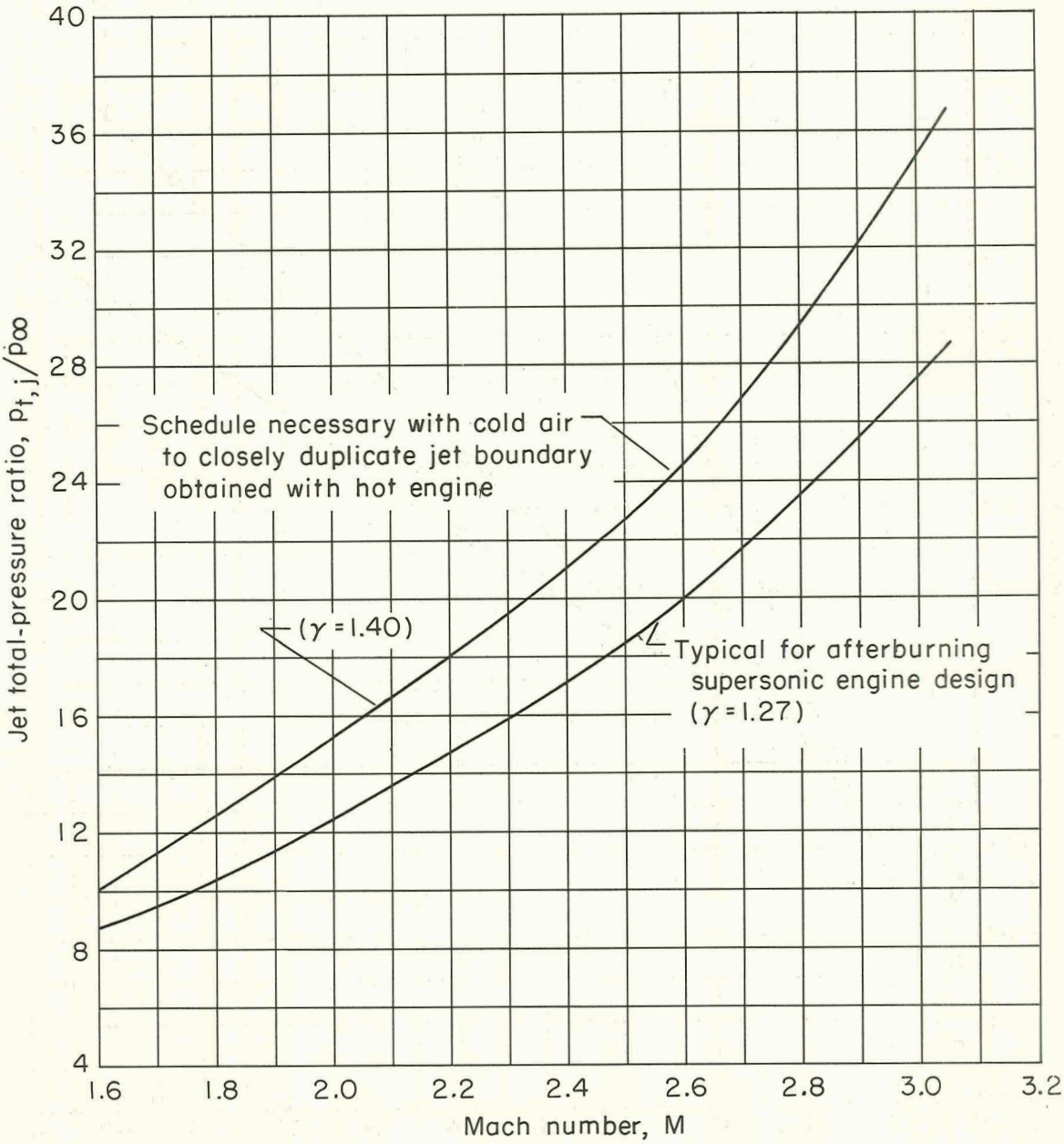

Figure 6.- Comparison between jet-total-pressure-ratio variation with Mach number for hot jet (γ = 1.27) and cold jet (γ = 1.40) which produce the same initial jet-boundary slope.

L-422

CONFIDENTIAL

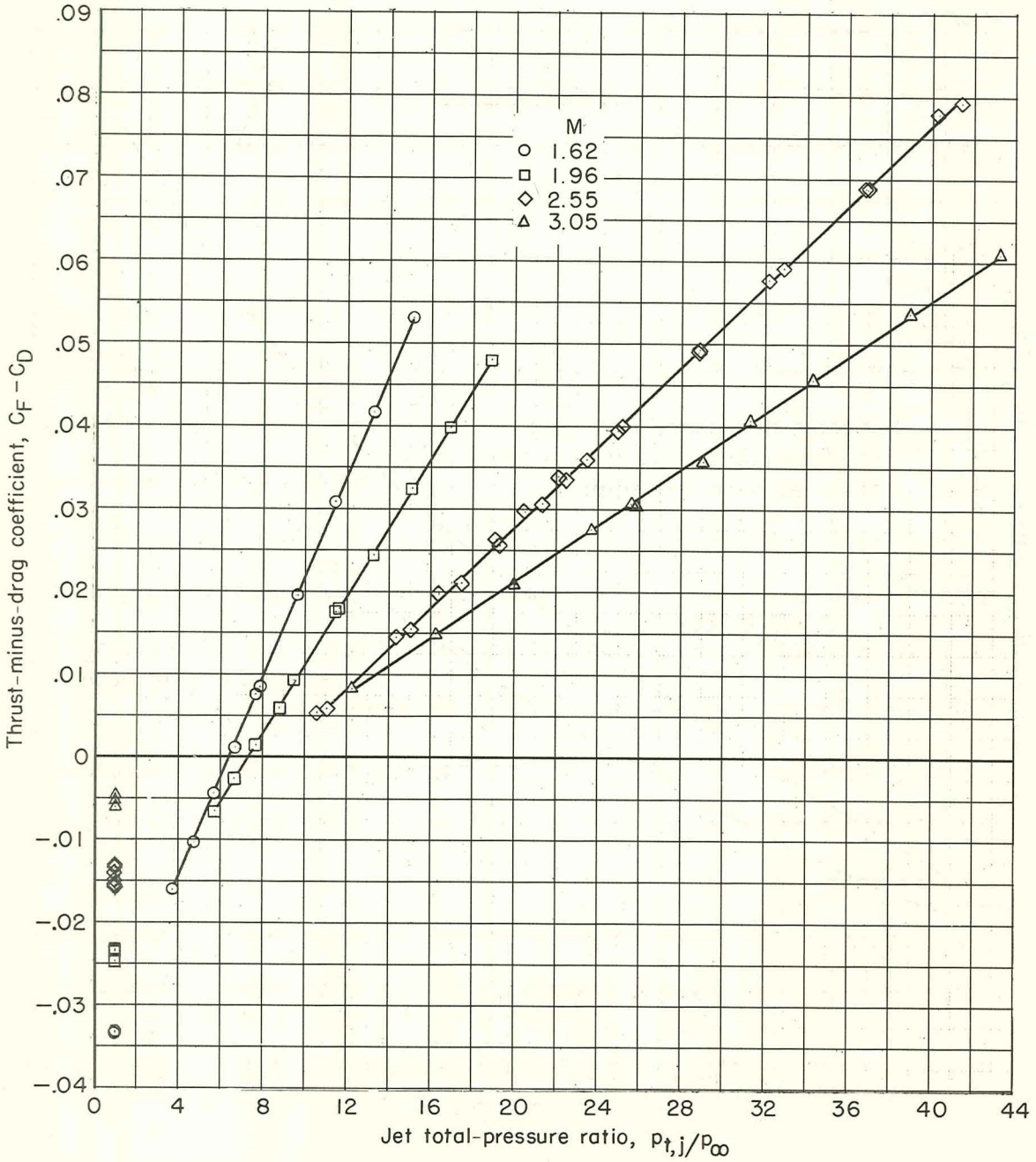

(a) Configuration 1.

Figure 7.- Effect of jet total-pressure ratio on measured thrust-minus-drag coefficient.

L-422

CONFIDENTIAL

L-422

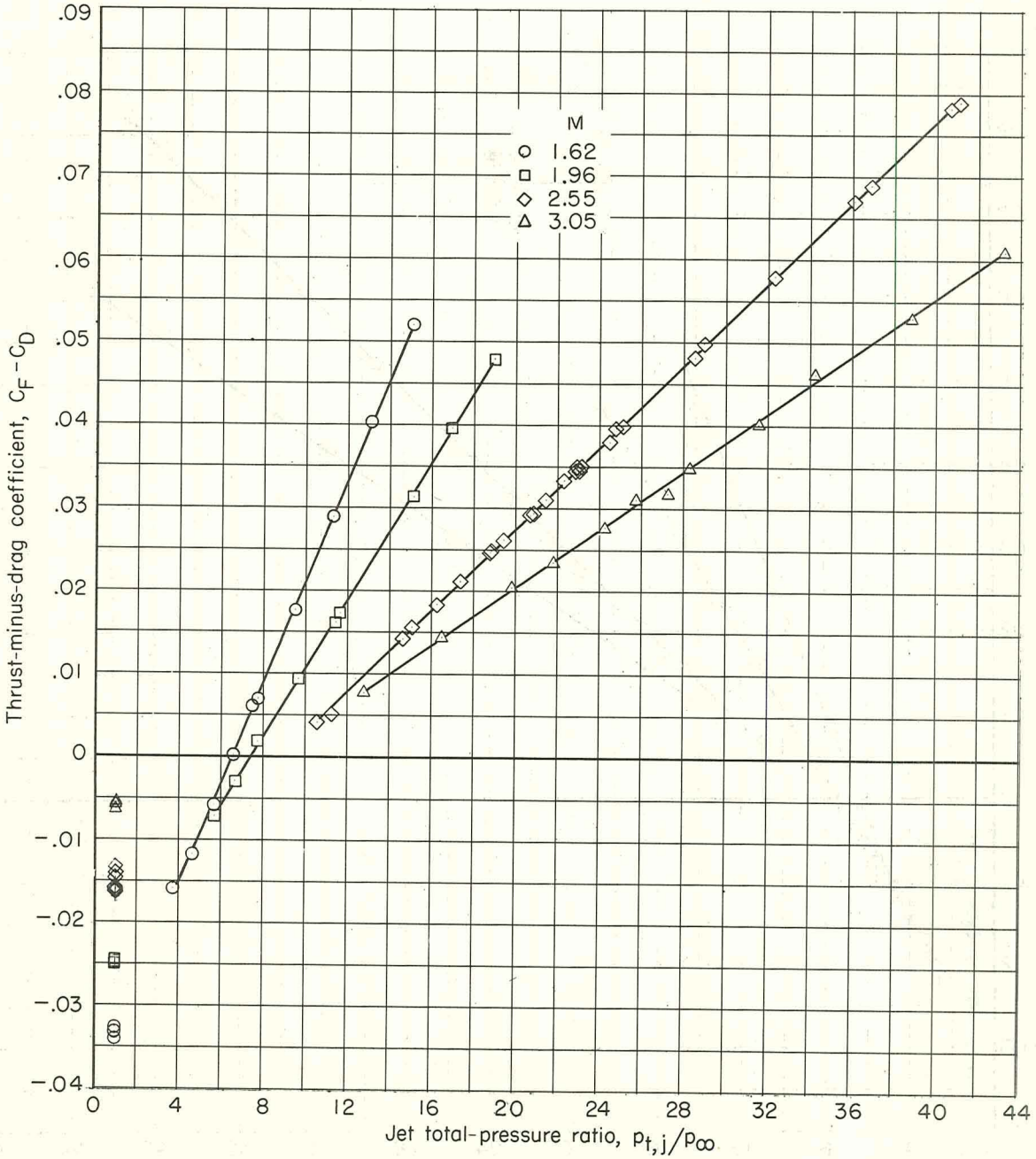

(b) Configuration 2.

Figure 7.- Continued.

CONFIDENTIAL

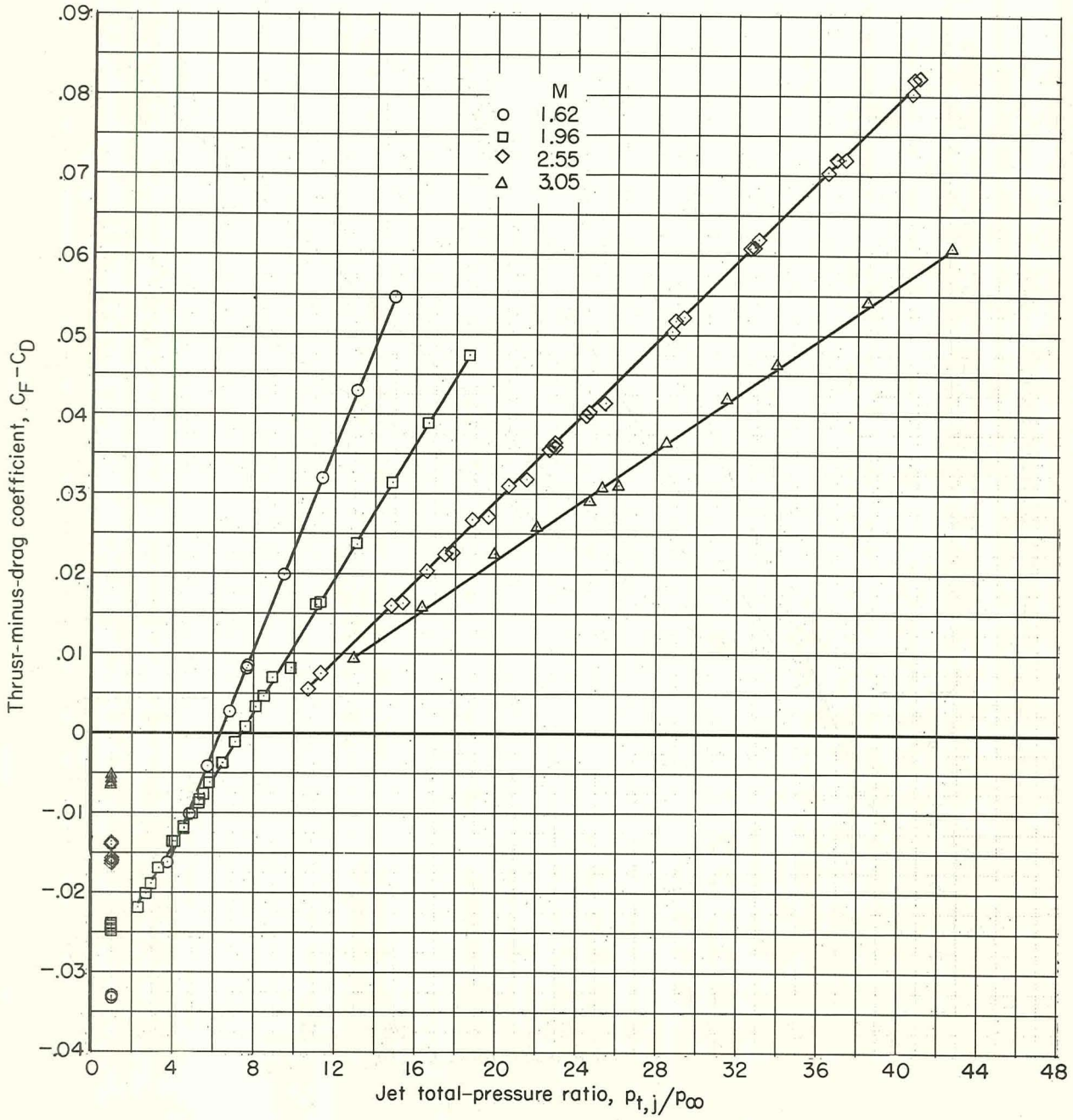

L-422

(c) Configuration 3.

Figure 7.- Continued.

CONFIDENTIAL

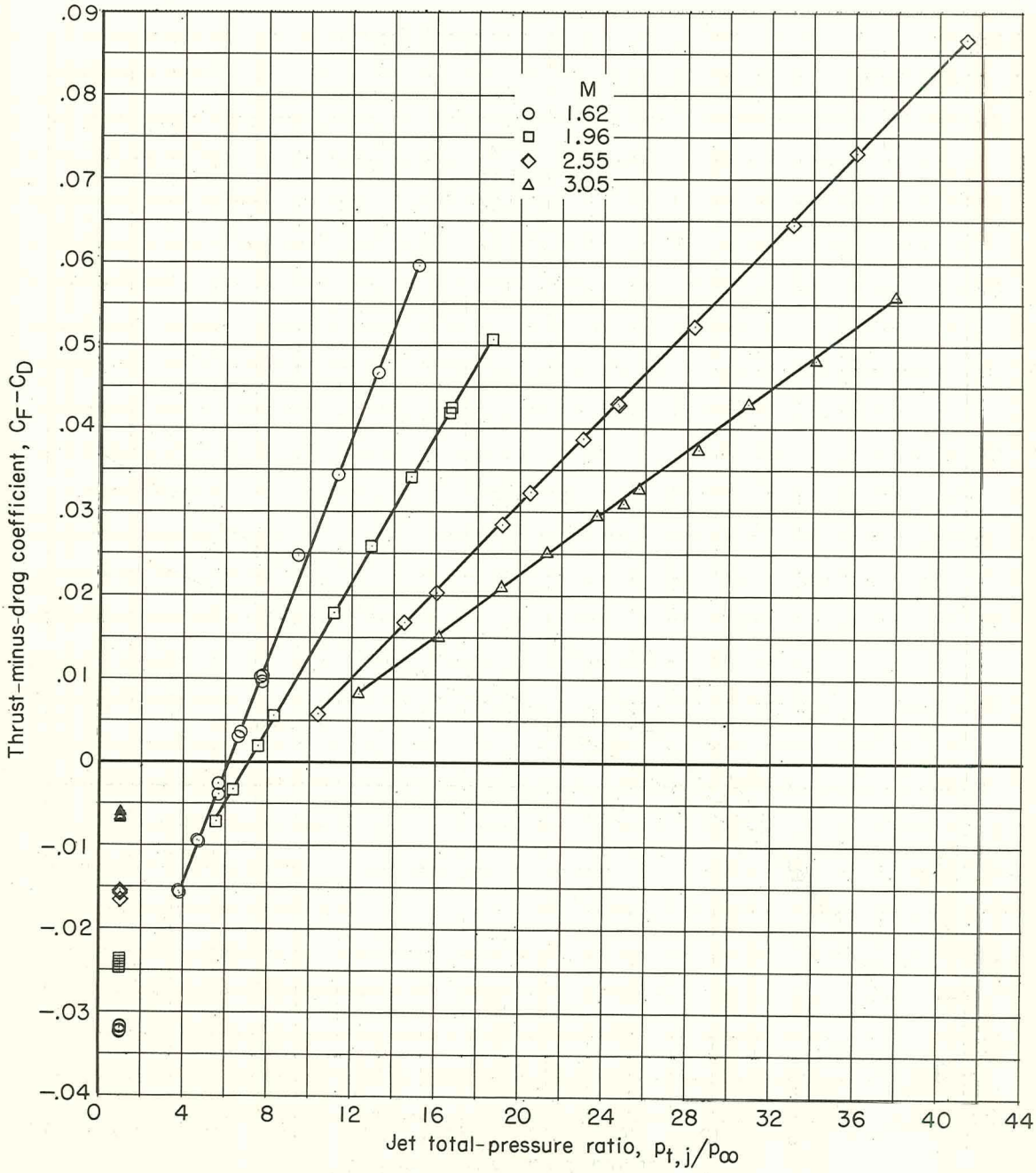

(d) Configuration 4.

Figure 7.- Continued.

CONFIDENTIAL

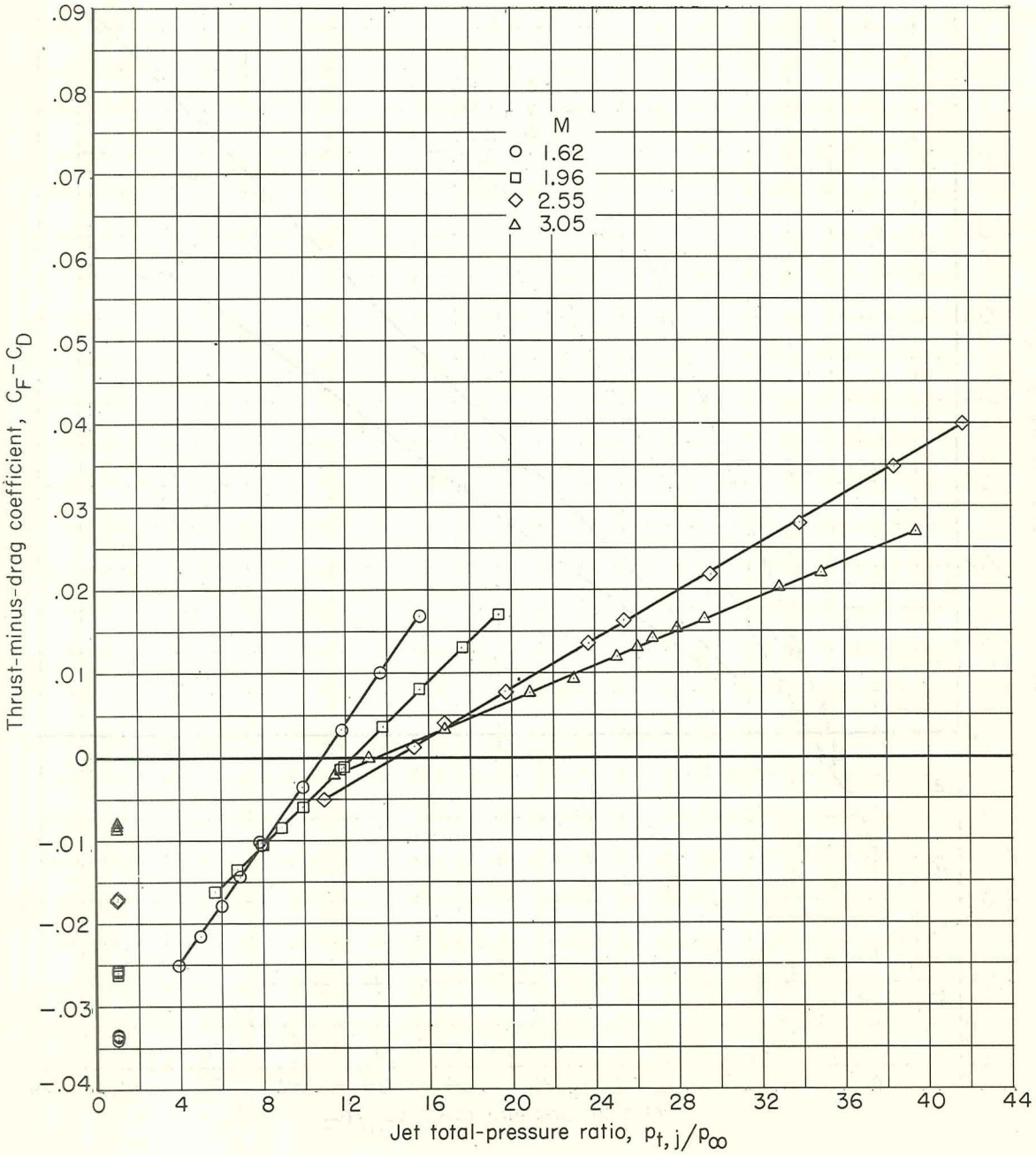

(e) Configuration 5.

Figure 7.- Continued.

CONFIDENTIAL

L-422

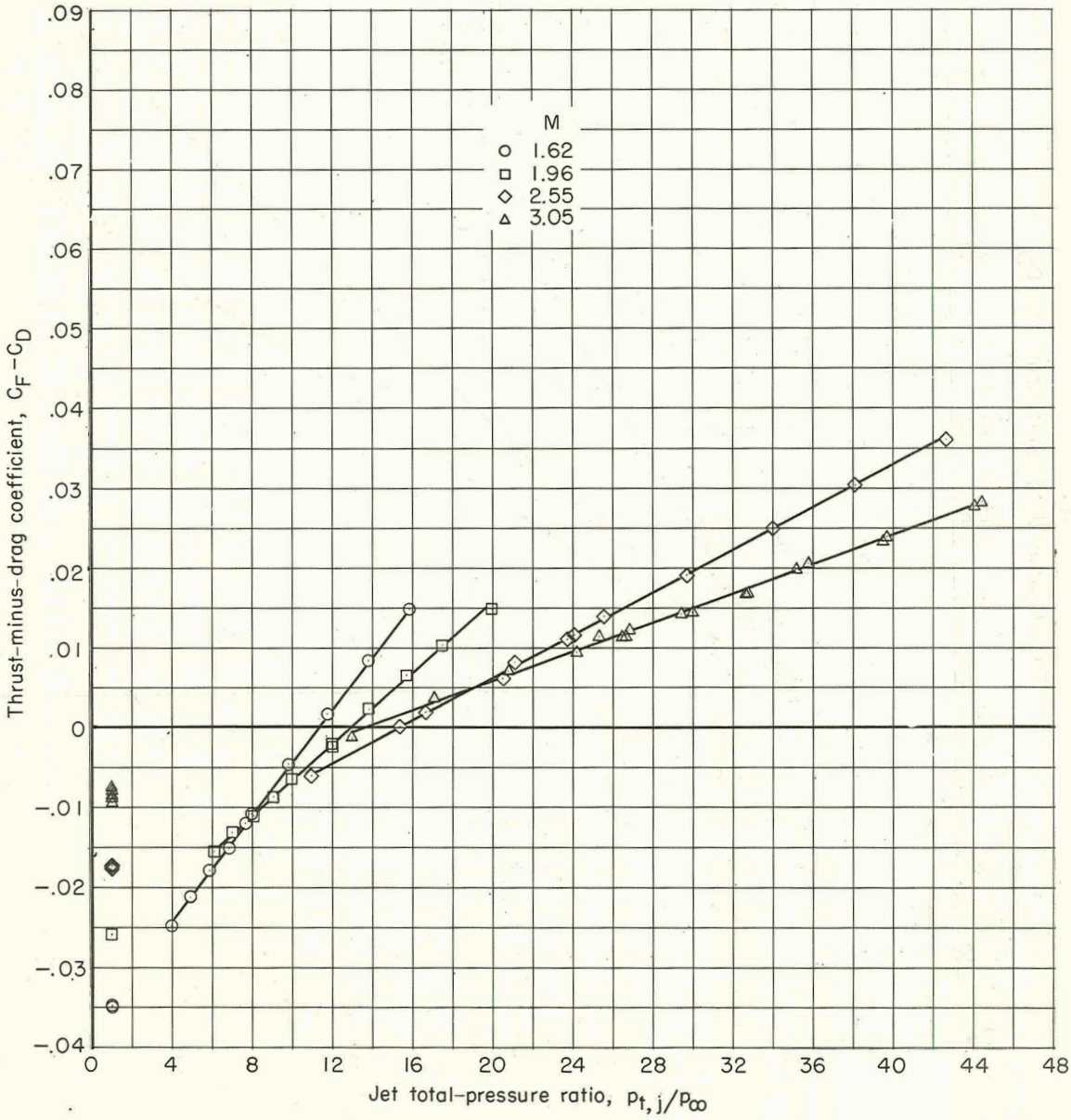

(f) Configuration 6.

Figure 7.- Continued.

[redacted]

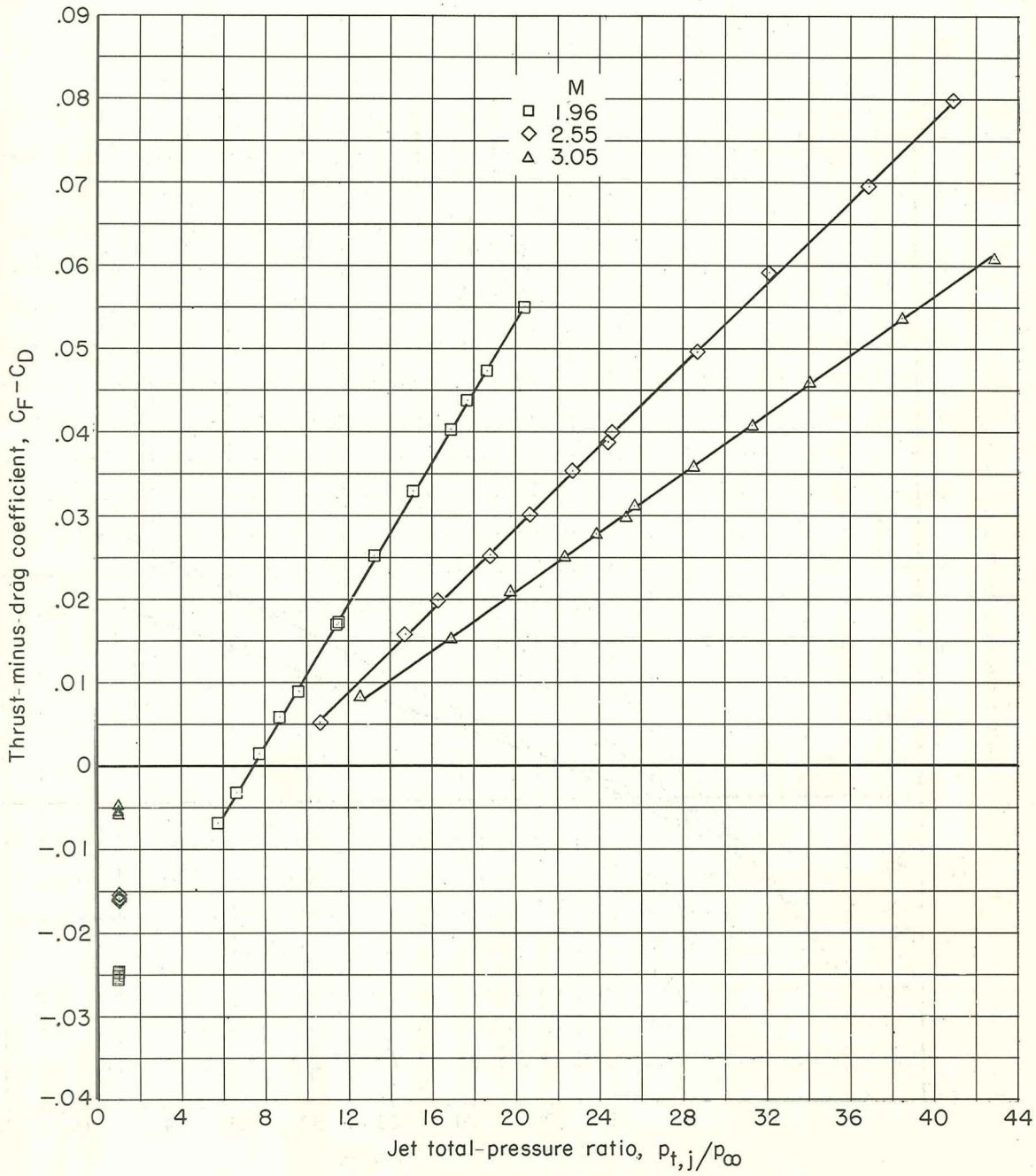

(g) Configuration 7.

Figure 7.- Continued.

[redacted]

L-422

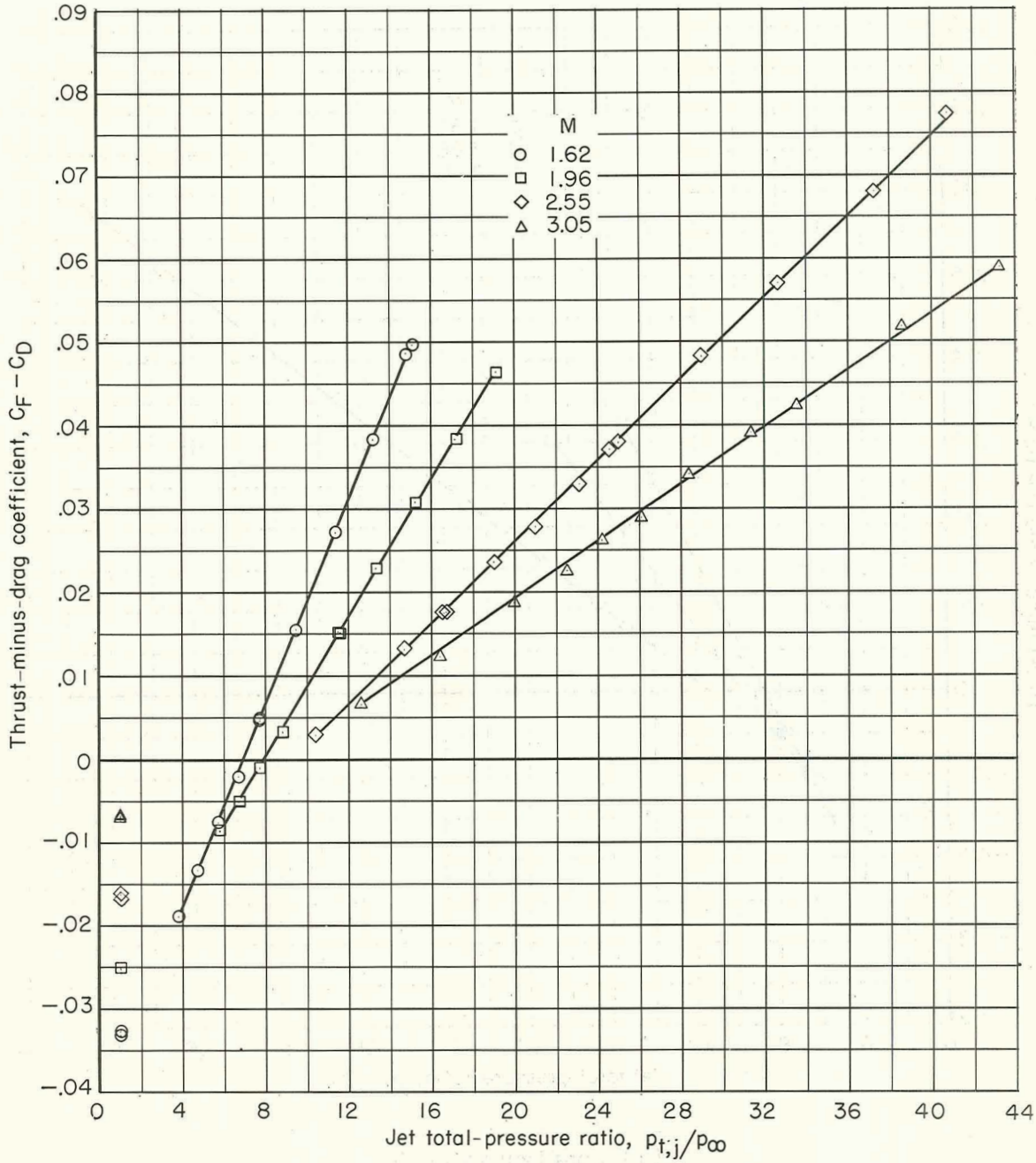

(h) Configuration 8.

Figure 7.- Continued.

CONFIDENTIAL

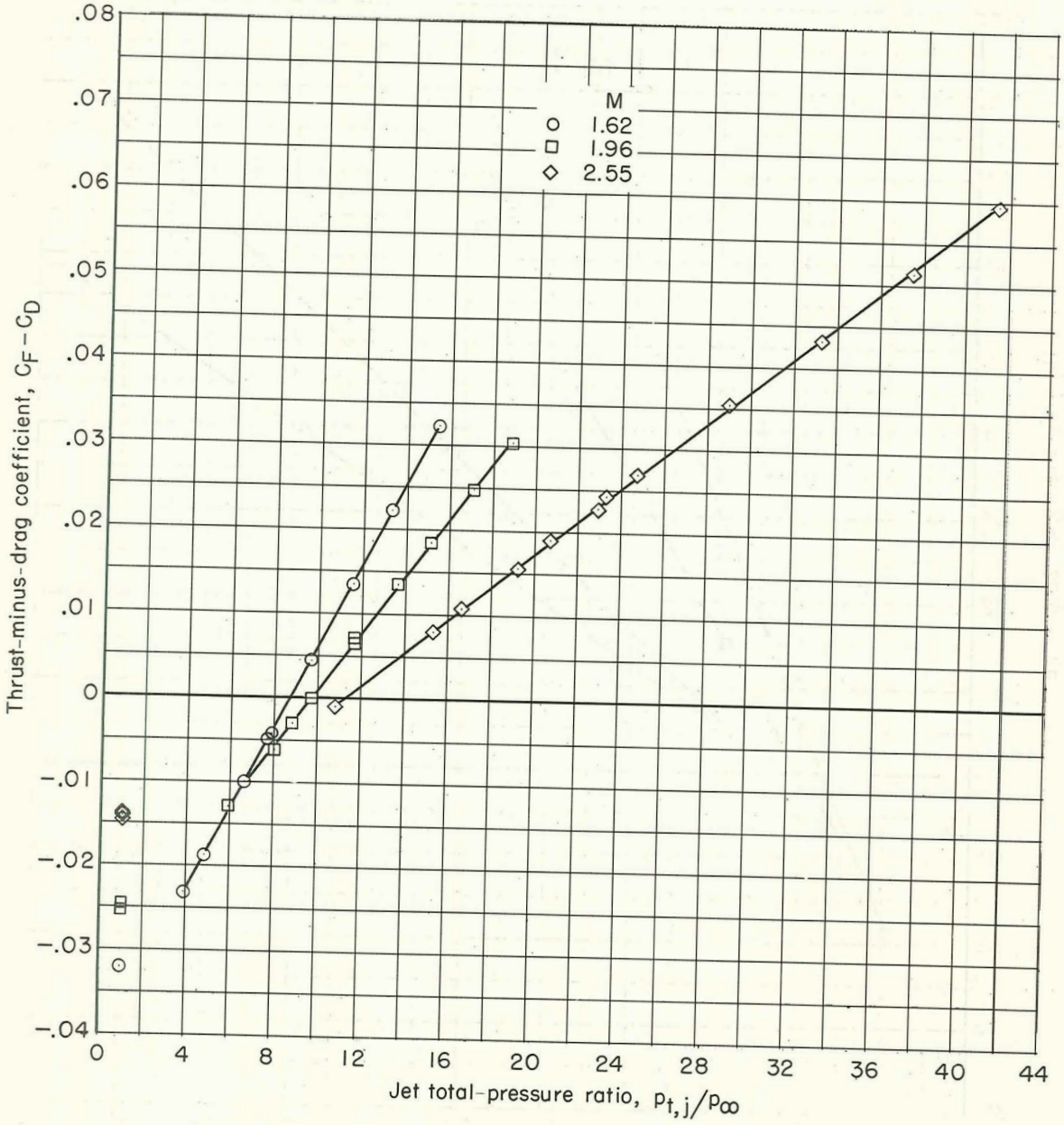

(i) Configuration 9.

Figure 7.- Concluded.

L-422

CONFIDENTIAL

L-422

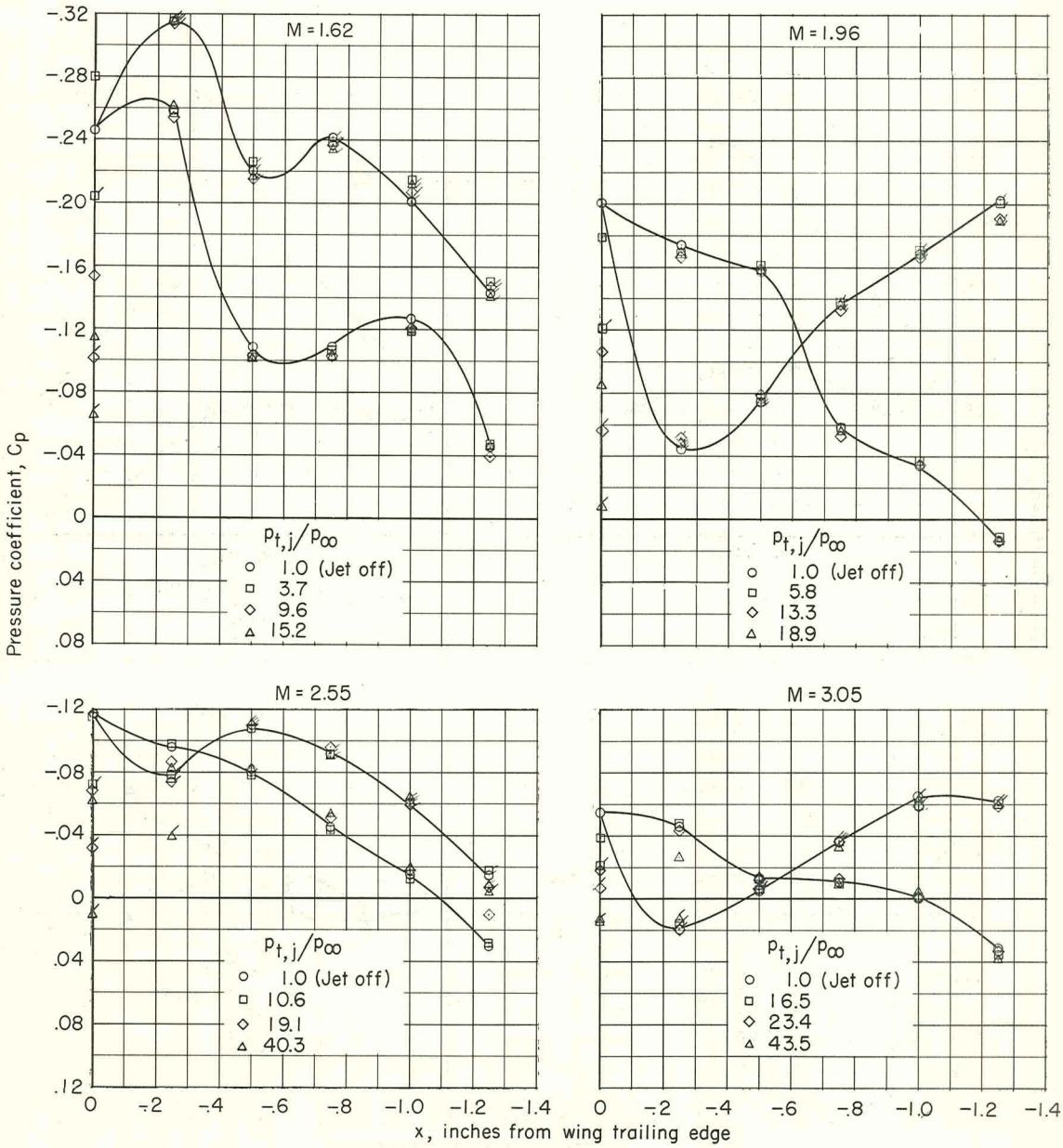

(a) Configuration 1.

Figure 8.- Variation of pressure coefficient along fairing between nacelles with distance from wing trailing edge. Flagged symbols are for lower surface.

CONFIDENTIAL

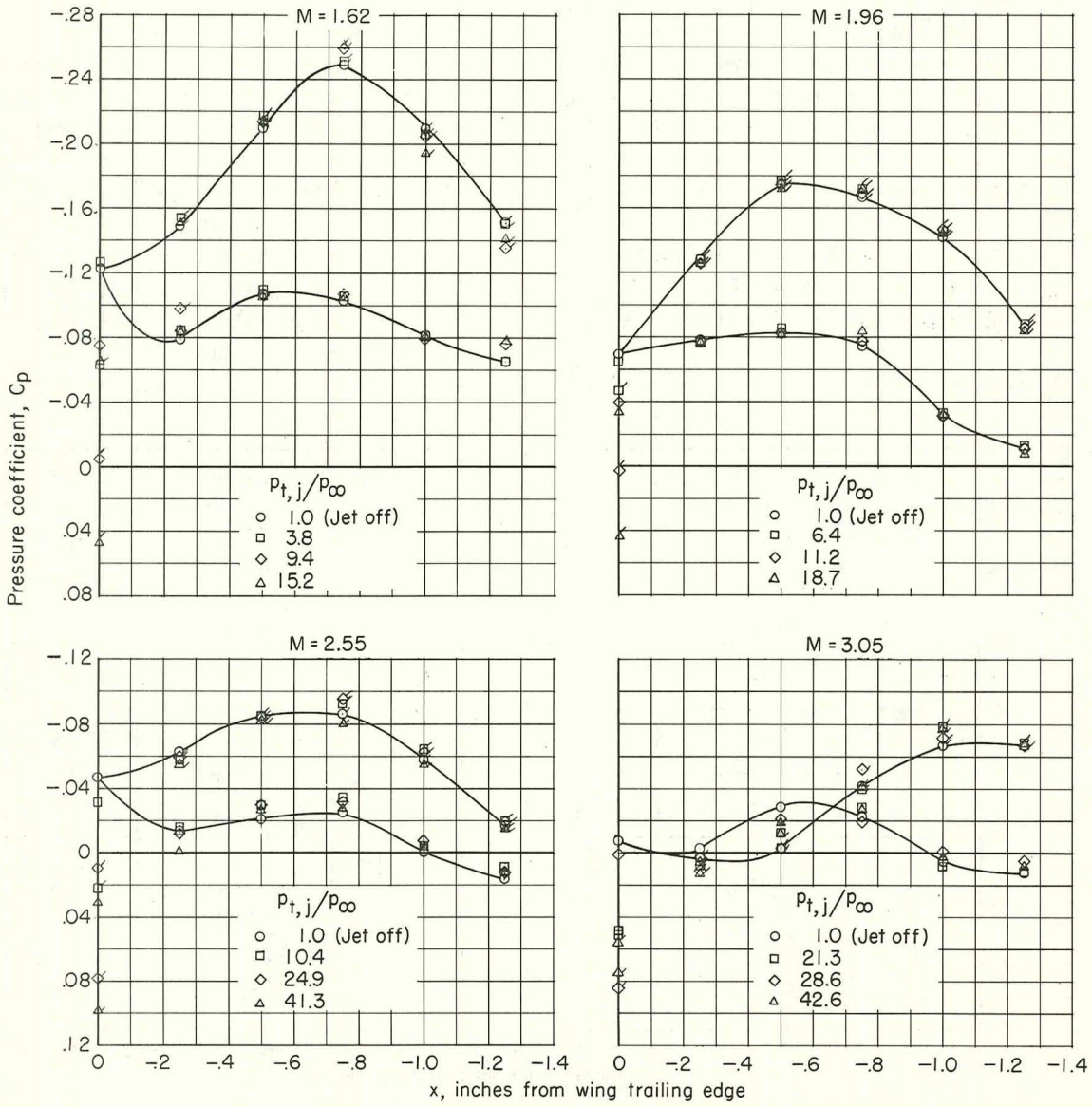

(b) Configuration 4.

Figure 8.- Concluded.

L-422

CONFIDENTIAL

CONFIDENTIAL

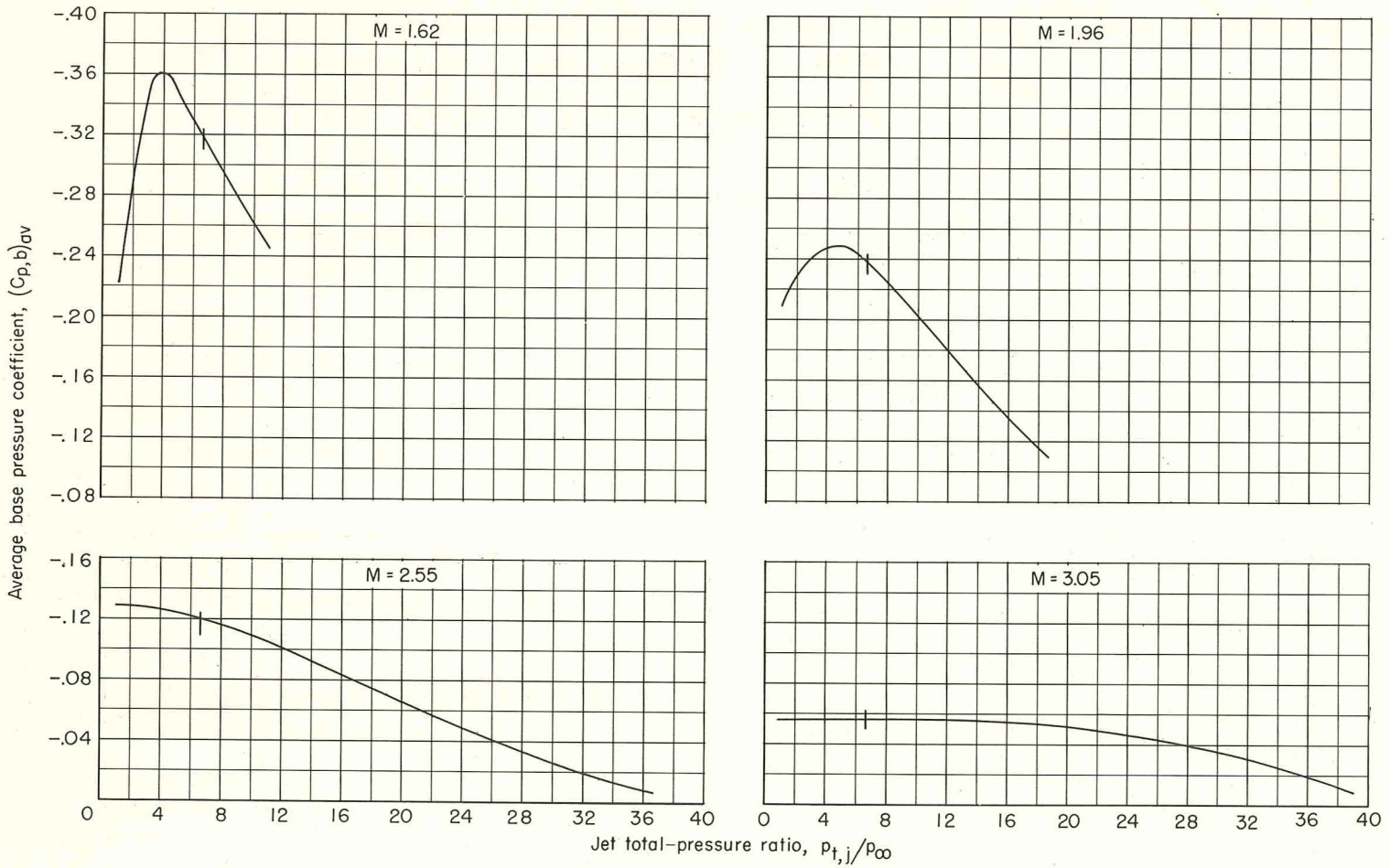

(a) Configuration 2.

Figure 9.- Effect of jet total-pressure ratio on average base pressure coefficient for several Mach numbers and configurations. Ticks indicate nozzle design pressure ratio (hot).

CONFIDENTIAL

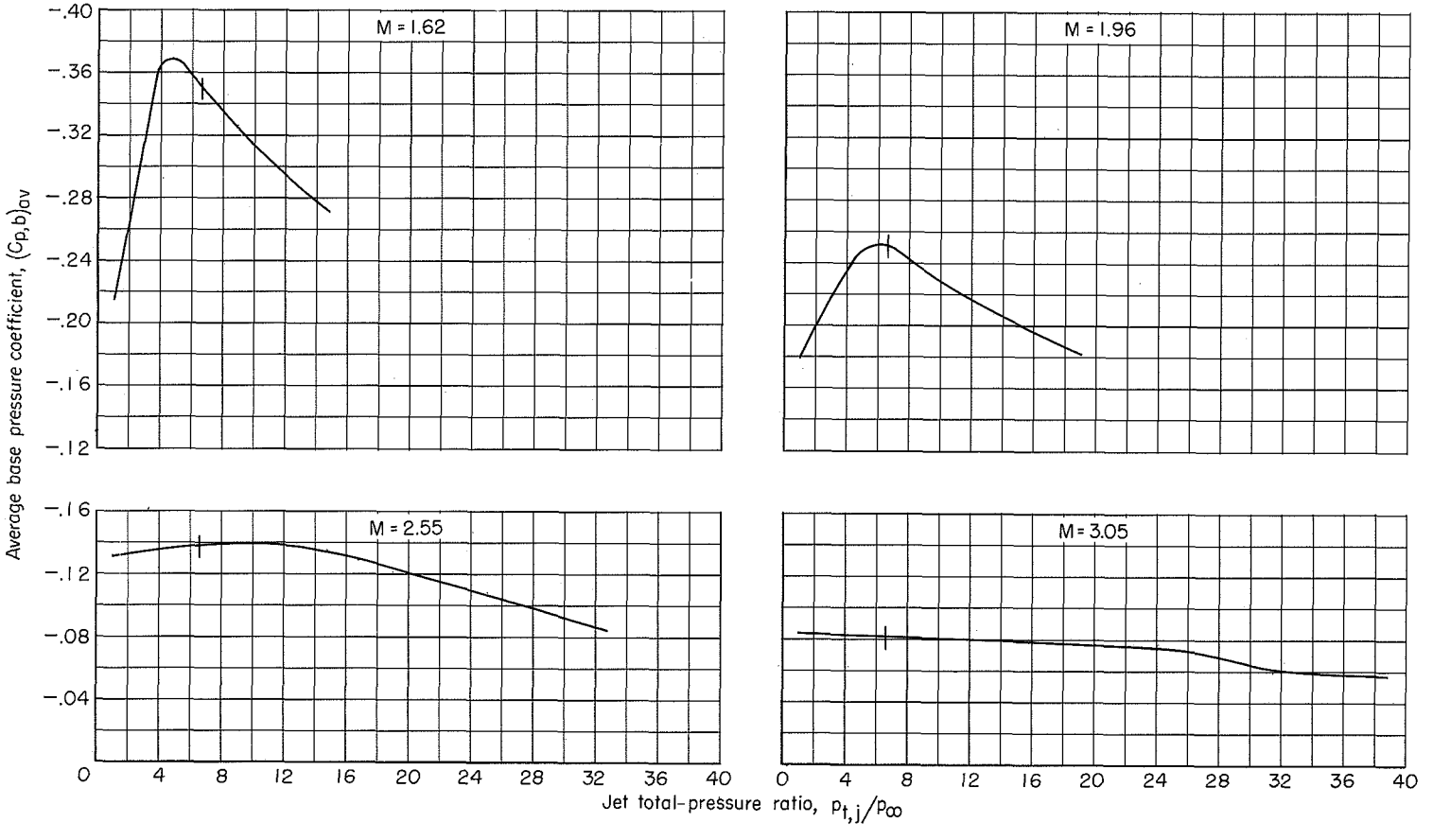

(b) Configuration 8.

Figure 9.- Continued.

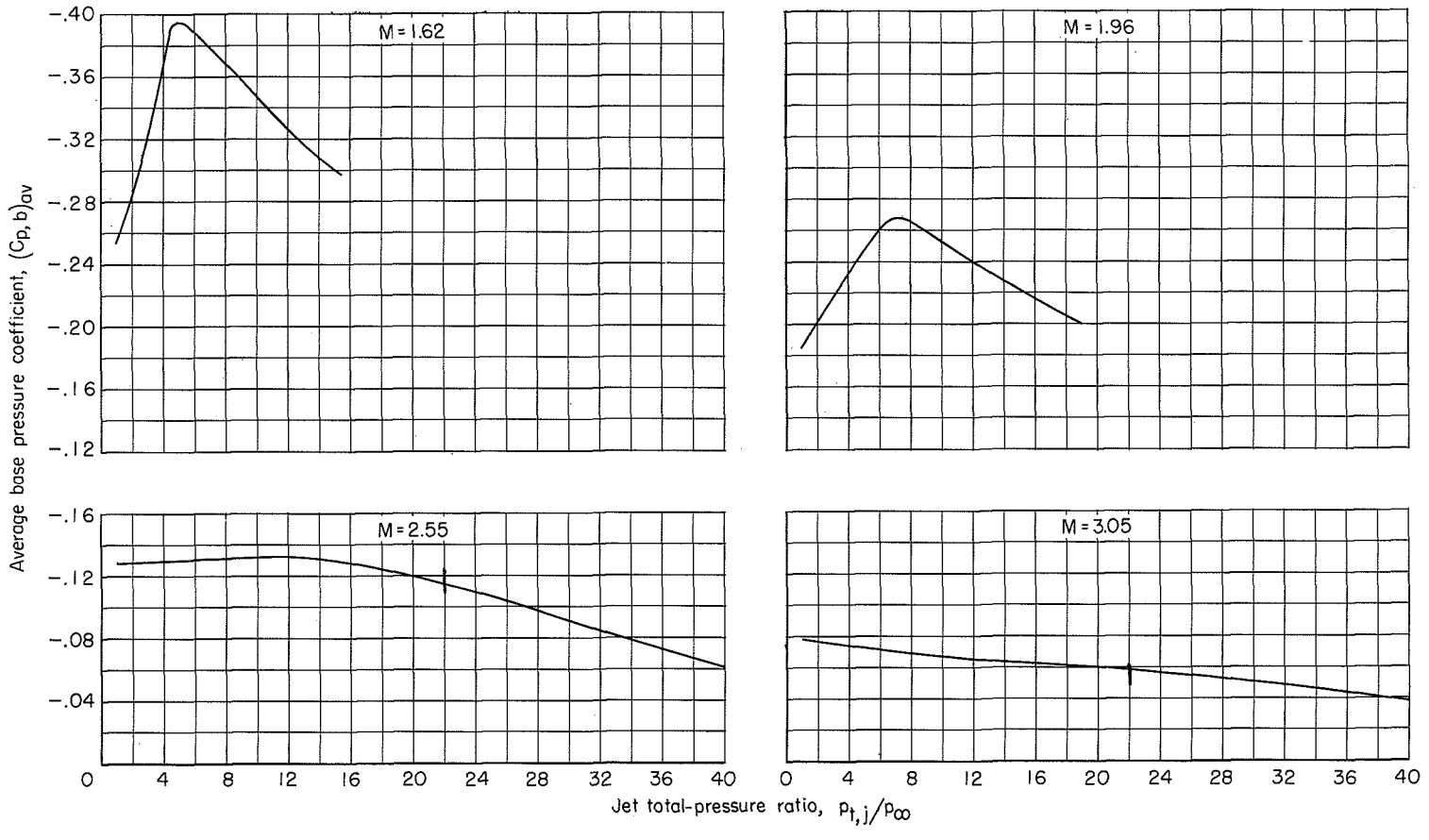

(c) Configuration 9.

Figure 9.- Concluded.

CONFIDENTIAL

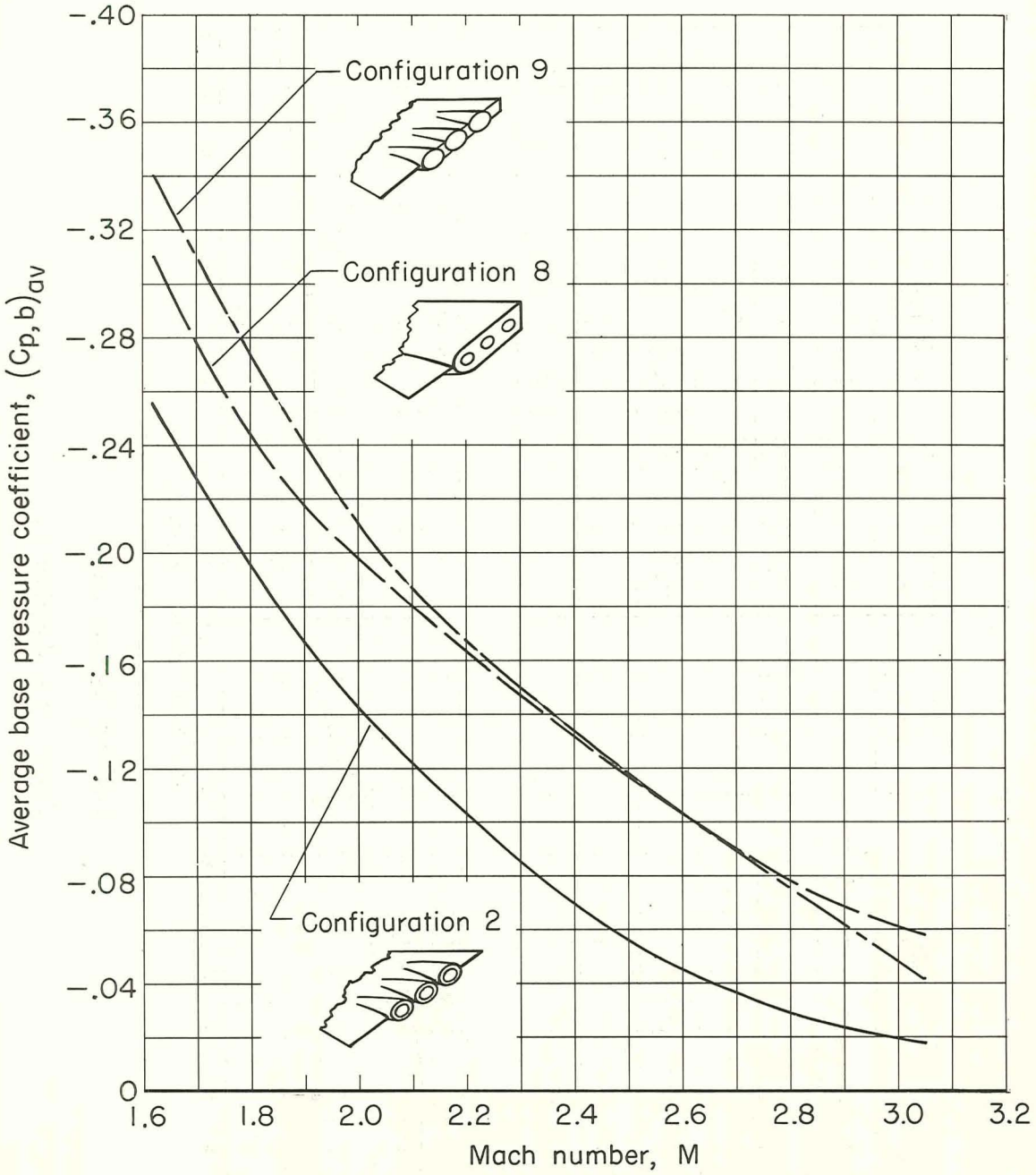

Figure 10.- Comparison of average base pressure coefficients with Mach number for three configurations for scheduled variation of jet total-pressure ratio.

CONFIDENTIAL

CONFIDENTIAL

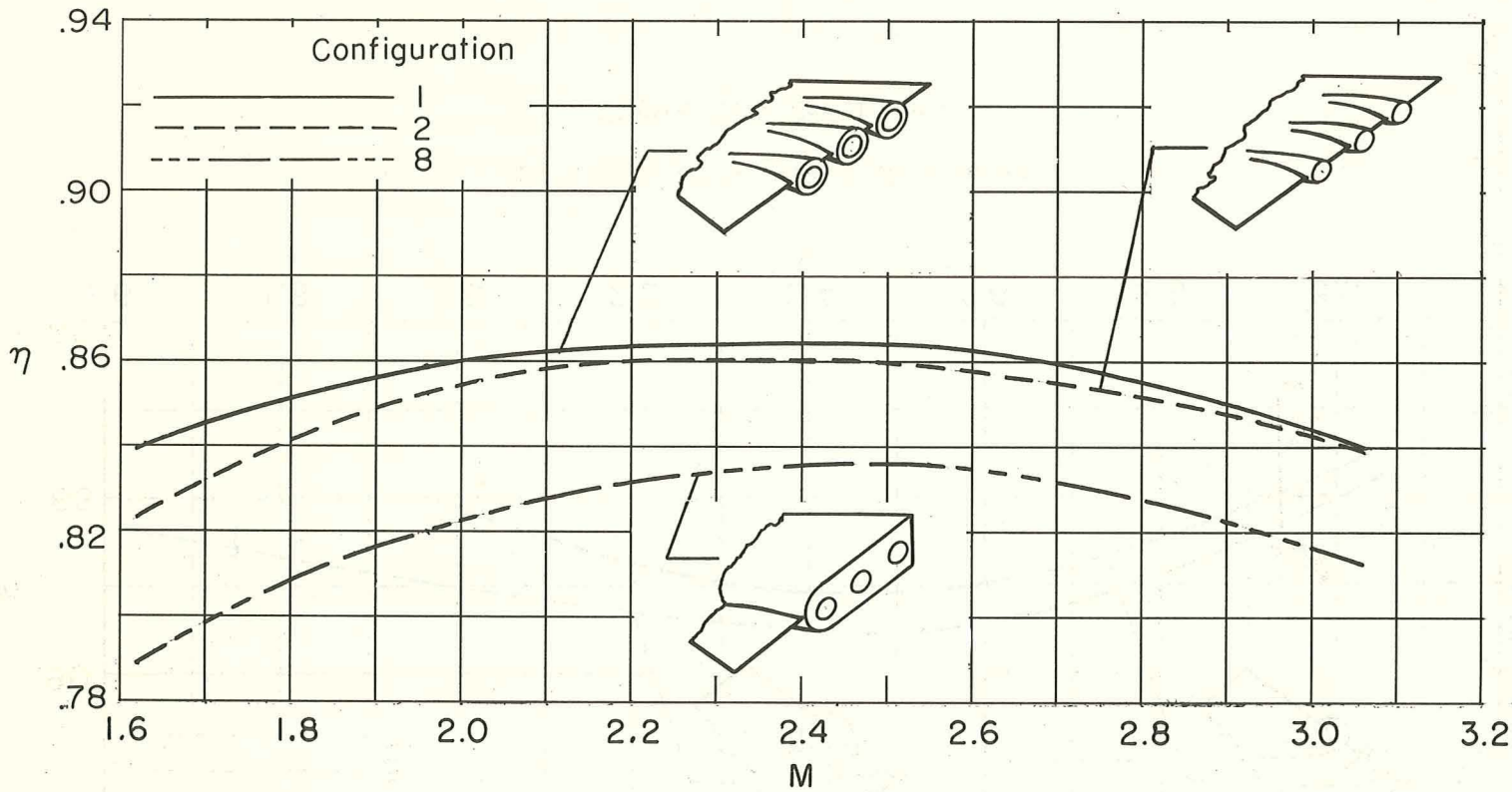

(a) Boattail compared with base area.

Figure 11.- Effect of Mach number on configuration efficiency factor. Data are for pressure ratio schedule for cold air shown in figure 6. Ticks indicate Mach number at which nozzle is on design pressure ratio.

CONFIDENTIAL

CONFIDENTIAL

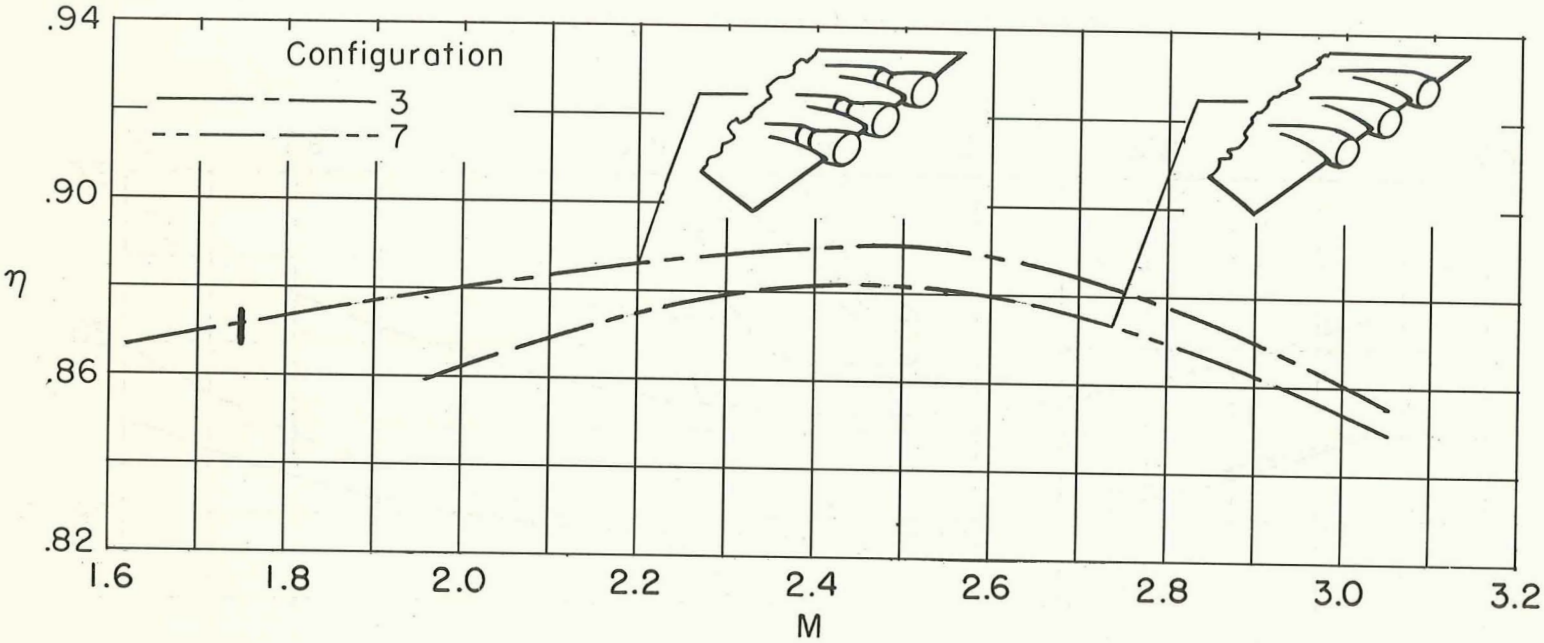

(b) Effect of boattail abruptness.

Figure 11.- Continued.

CONFIDENTIAL

CONFIDENTIAL

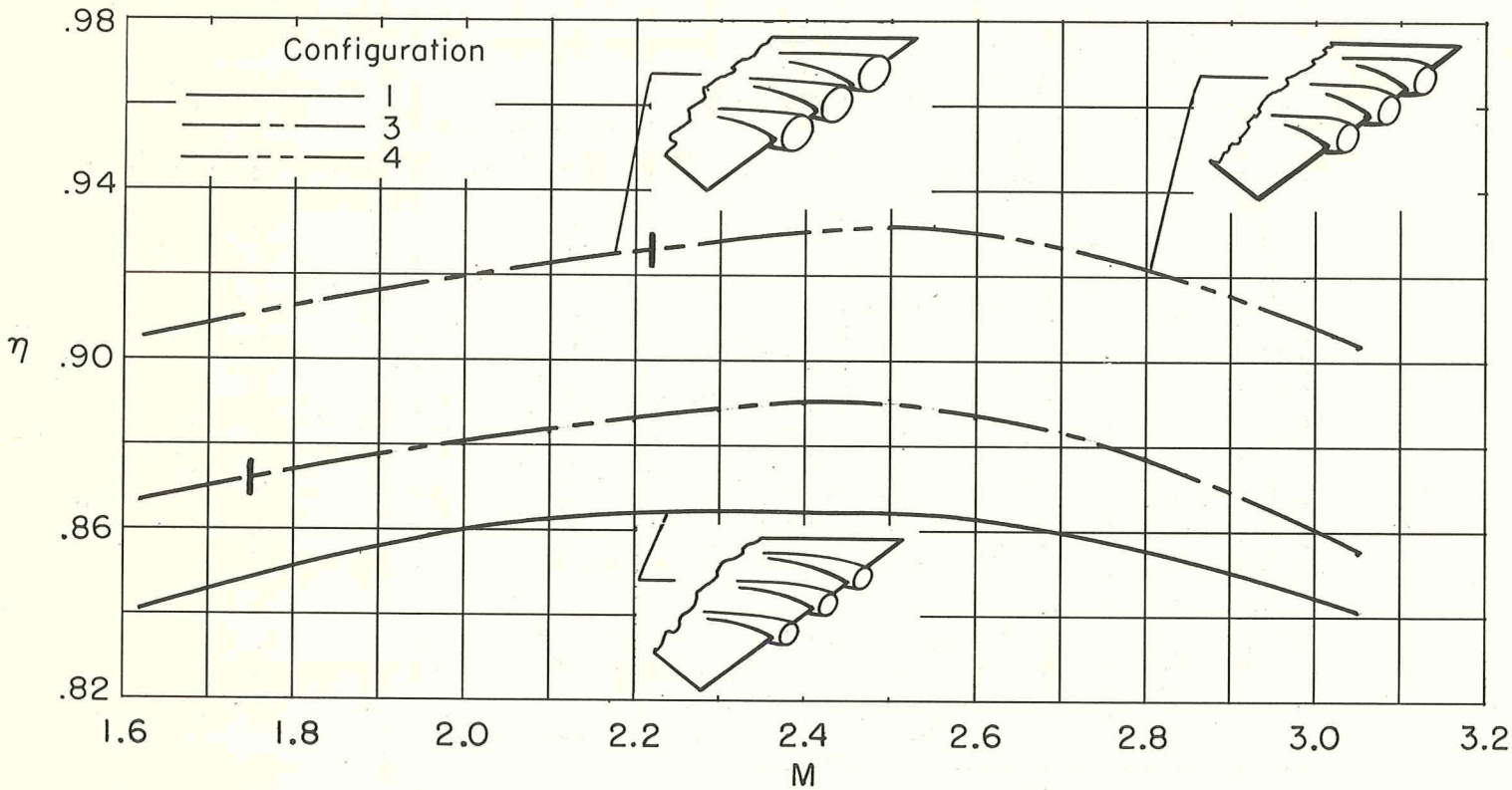

(c) Effect of simultaneous variation in nozzle external and internal geometry.

Figure 11.- Continued.

CONFIDENTIAL

CONFIDENTIAL

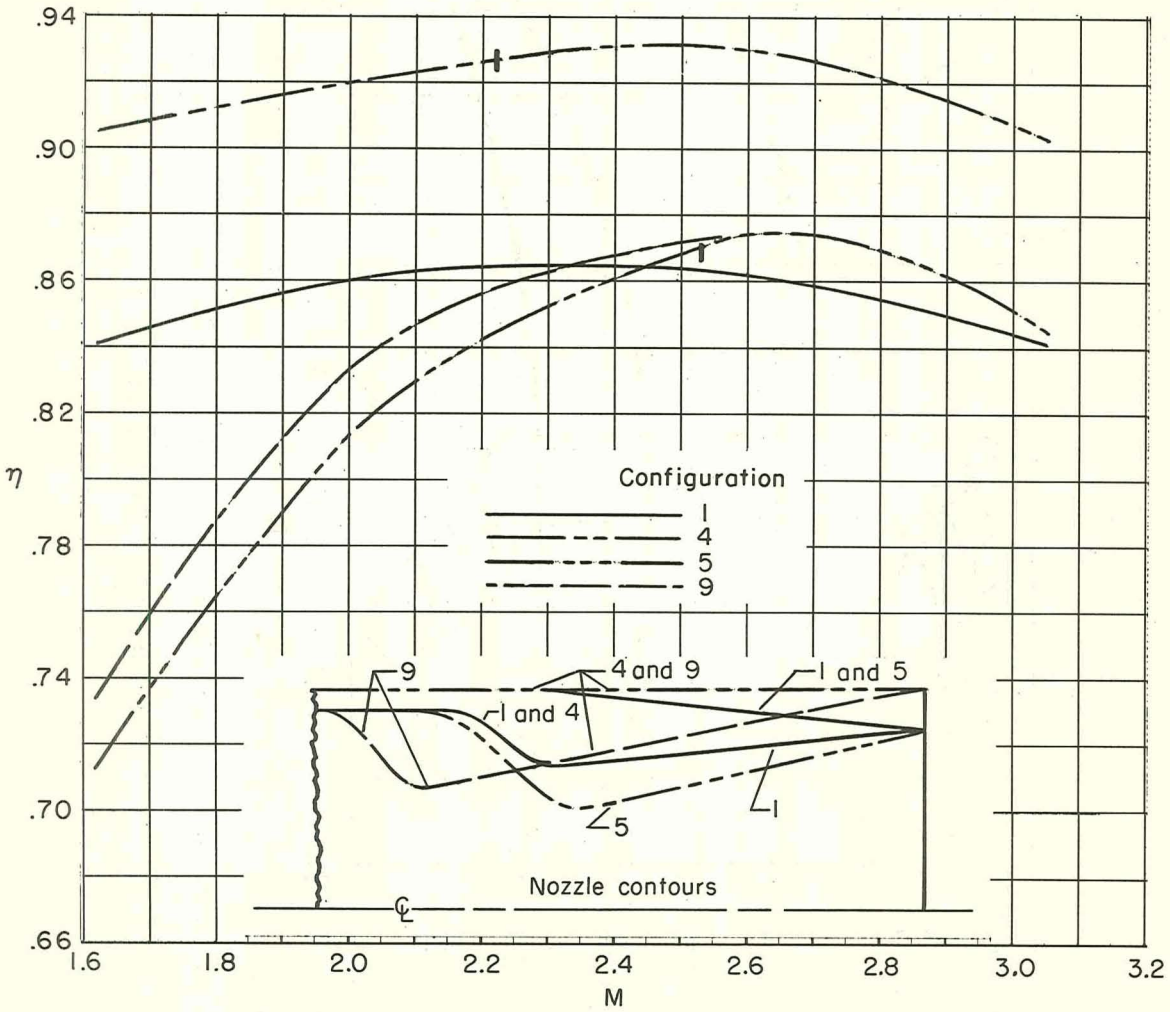

(d) Effect of increasing nozzle-area ratio.

Figure 11.- Concluded.

CONFIDENTIAL

CONFIDENTIAL

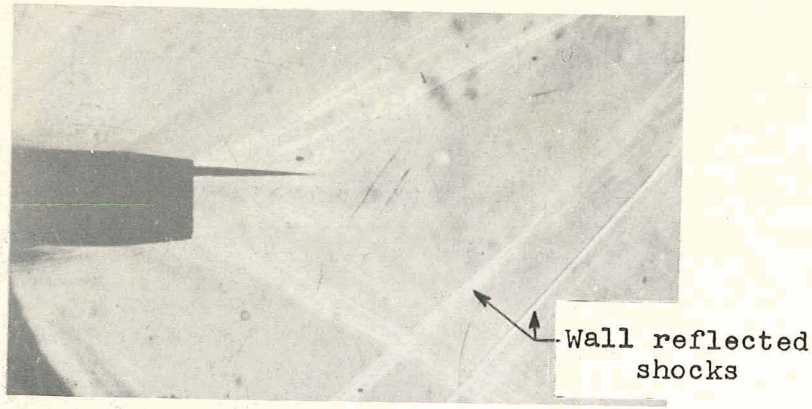

$M = 1.62$, $p_{t,j}/p_\infty = 6.7$

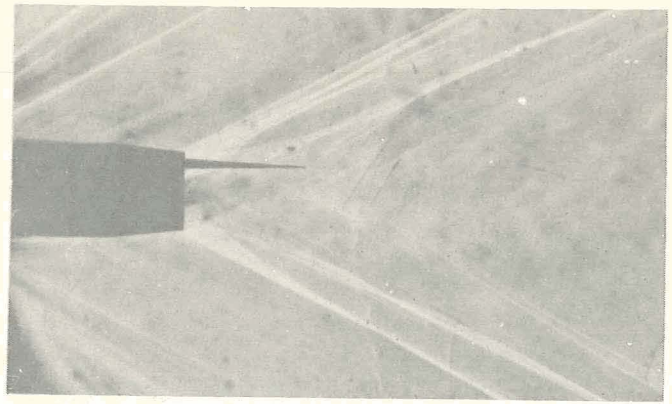

$M = 1.96$, $p_{t,j}/p_\infty = 11.6$

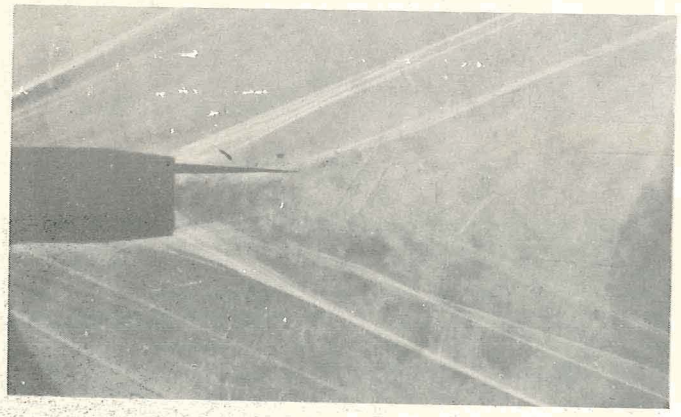

$M = 2.55$, $p_{t,j}/p_\infty = 20.5$

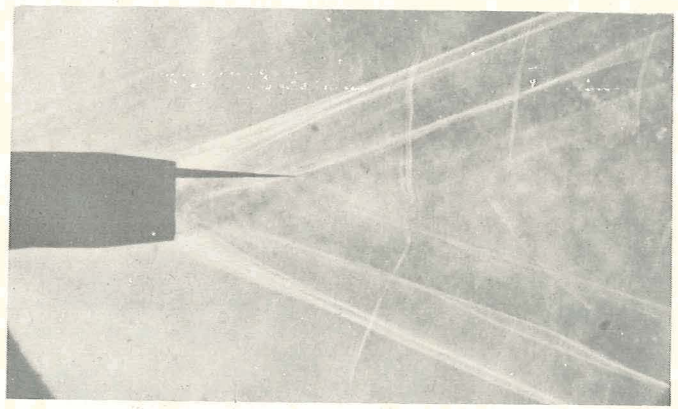

$M = 3.05$, $p_{t,j}/p_\infty = 31.3$

(a) Configuration 1.

L-59-229

Figure 12.- Schlieren photographs of several configurations.

CONFIDENTIAL

CONFIDENTIAL

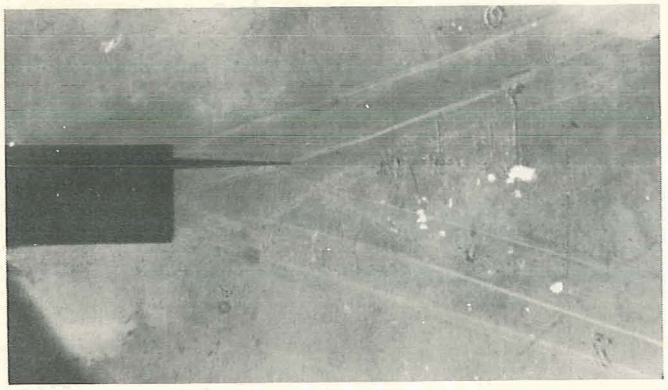

Configuration 2

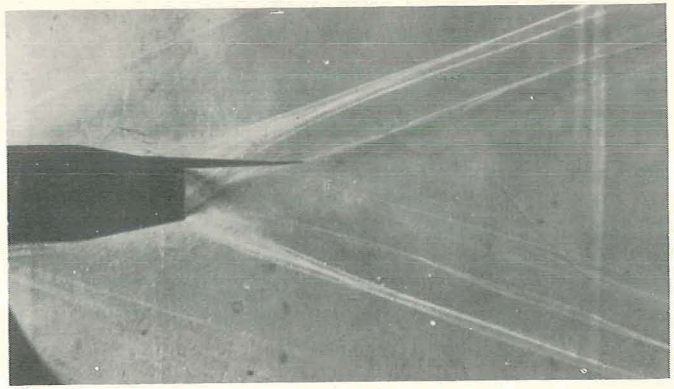

Configuration 6

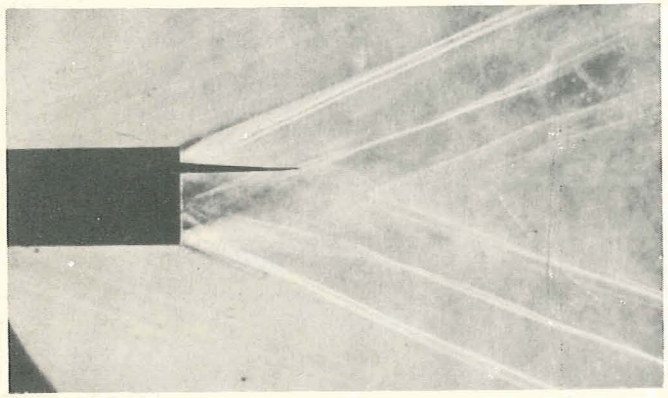

Configuration 8

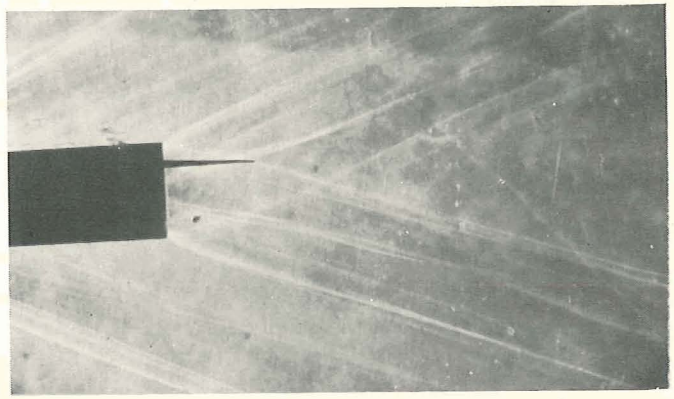

Configuration 9

(b) Configurations 2, 6, 8, and 9. $M = 3.05$; $p_{t,j}/p_\infty \approx 32$. L-59-230

Figure 12.- Concluded.

CONFIDENTIAL

NASA - Langley Field, Va. L-422

CONFIDENTIAL

CONFIDENTIAL